POLITECNICO DI TORINO

MASTER's Degree in BIOMEDICAL ENGINEERING

Evaluating the Effects of Active Ankle-Foot Orthoses on Achilles Tendon Load in Gait Rehabilitation

A Comparative Musculoskeletal Study

Supervisors

Prof. Danilo DEMARCHI

Prof. Paolo BONATO

Dr. Giulia CORNIANI

Candidate

Alessandro COLUCCI

2024/2025

POLITECNICO DI TORINO

MASTER's Degree in BIOMEDICAL ENGINEERING

Evaluating the Effects of Active Ankle-Foot Orthoses on Achilles Tendon Load in Gait Rehabilitation

A Comparative Musculoskeletal Study

Supervisors

Prof. Danilo DEMARCHI

Prof. Paolo BONATO

Dr. Giulia CORNIANI

Candidate

Alessandro COLUCCI

2024/2025

Abstract

The Achilles tendon (AT) is the strongest tendon in the human body, playing a critical role in gait by transmitting forces from the triceps surae (gastrocnemius and soleus muscles) to enable plantarflexion. Despite its strength, the AT is highly susceptible to injury due to the repetitive high-load stresses it endures during locomotor activities such as walking and running.
Rehabilitation following Achilles tendon rupture or surgical repair is often prolonged and complex. Traditional protocols based on joint immobilization can lead to persistent deficits in plantarflexor strength, proprioception, and tendon stiffness, primarily due to adverse changes in muscle-tendon morphology and function—particularly affecting the soleus muscle.

Active ankle-foot orthoses (AFOs) have emerged as promising tools for facilitating active rehabilitation by delivering controlled assistance that can offload the Achilles tendon and support functional recovery. By generating assistive torque in response to gait events, these devices can provide adaptive support tailored to the individual needs of the recovery process. Still, evaluating their effectiveness remains challenging due to the lack of feasible in vivo techniques for measuring AT force during dynamic movement. Invasive methods are not clinically viable, and non-invasive options like tensiometry are limited by placement complexity and postprocessing demands. Consequently, musculoskeletal modeling has become a scalable and accessible method for estimating AT load and assessing the biomechanical effects of such devices.

This study aims to investigate the interaction between active AFO support and the musculoskeletal system to inform more effective rehabilitation strategies for lower limb injuries. To this end, we conducted a comparative musculoskeletal modeling analysis to estimate Achilles tendon (AT) loading during walking across five experimental conditions: walking without an AFO, with a passive AFO, and with three increasing levels of powered assistance.
Surface electromyography (sEMG), kinetic, and kinematic data were collected from 11 healthy subjects walking at two speeds. Two simulation platforms, OpenSim and MyoSuite, were used to process the experimental data and estimate joint kinematics, muscle activations, and AT forces across conditions. Full time series and summary metrics were analyzed, with inverse kinematics results validated against motion capture data. Results showed strong agreement between platforms in estimating hip, knee, and ankle angles.

Focus was placed on the Triceps Surae and Tibialis Anterior muscles, whose activation levels, recorded via sEMG and modeled through simulation, served as indirect indicators of AT loading. Results showed that higher powered assistance levels were associated with reduced muscle activation and tendon forces, supporting the potential of robotic AFOs to lower the mechanical demand on the Achilles tendon

during gait.

These findings underscore the potential of powered AFOs as tools for active rehabilitation targeting tendon recovery. Additionally, this work highlights the value of simulation-based musculoskeletal modeling using OpenSim and MyoSuite to inform both biomechanical research and clinical decision-making.

ACKNOWLEDGMENTS

I would like to express my deepest gratitude to Prof. Paolo Bonato, my supervisor at Spaulding Rehabilitation Hospital, Harvard Medical School. His vision, expertise, and continuous support have been pivotal to the development and completion of this thesis. I am truly honored to have conducted my research under his guidance in such a distinguished and inspiring environment.

I am equally thankful to Prof. Danilo Demarchi from Politecnico di Torino, who made this extraordinary opportunity possible by supporting my research placement in Boston. His trust and encouragement have been fundamental in shaping both my academic path and professional growth.

A special thank you goes to Dr. Giulia Corniani, whose mentorship and dedicated supervision guided me through every stage of this project. Her patience, insightful feedback, and constant availability have been invaluable, both scientifically and personally.

I am also grateful to Dr. Vittorio Caggiano for providing crucial perspectives and support from the industrial side, significantly enriching the scope of this work.

I would like to extend my appreciation to Dr. Giulio Rigoni for his indispensable help with data processing and technical discussions, as well as to all the members of the Motion Analysis Lab at Spaulding Rehabilitation Hospital for their assistance, collaboration, and for creating such a welcoming, fun and stimulating environment.

Finally, I wish to express my heartfelt gratitude to my family and friends for their unwavering support, understanding, and encouragement throughout this journey. Their presence has been a source of strength and motivation at every step.

To my family.

Table of Contents

List of Figures

List of Tables

Acronyms

AFO	Ankle Foot Orthoses.
AMTI	Advanced Mechanical Technology Inc..
AT	Achilles Tendon.
ATF	Achilles Tendon Force.
BTK	Biomechanical ToolKit.
CMC	Computed Muscle Control.
CMC (Corr)	Coefficient of Multiple Correlation.
CMC-EMG	EMG-informed Computed Muscle Control.
CoM	Center of Mass.
DoF	Degree of Freedom.
EMG	Electromyography.
FE	Flexion/Extension.
GRF	Ground Reaction Forces.
ID	Inverse Dynamics.
IK	Inverse Kinematics.
IOR	Istituto Ortopedico Rizzoli.
IRB	Institutional Review Board.
MSK	Musculoskeletal.
MTU	Muscle-Tendon Unit.
MVC	Maximum Voluntary Contraction.
NRMSE	Normalized Root Mean Square Error.
PD	Proportional-Derivative (control).

RMSE	Root Mean Square Error.
ROM	Range Of Motion.
RRA	Residual Reduction Algorithm.
SD	Standard Deviation.
SNRC	Spaulding National Running Center.
SHC	Spaulding Hospital Cambridge.

Chapter 1

The Motion Analysis Lab

The **Motion Analysis Lab (MAL)** is a state-of-the-art research facility located at Spaulding Rehabilitation Hospital in Boston, Massachusetts. Operated in collaboration with the *Department of Physical Medicine and Rehabilitation at Harvard Medical School*, the lab focuses on the quantitative assessment of human movement, with applications in rehabilitation, assistive technology, and neuromuscular biomechanics. Equipped with advanced instrumentation, including marker-based motion capture systems, instrumented treadmills, force platforms, and wearable sensors, the MAL supports both clinical and research investigations aimed at improving functional outcomes in individuals with neurological and musculoskeletal disorders. The interdisciplinary nature of the lab fosters collaborations among clinicians, engineers, and scientists, providing an ideal environment for the development and validation of innovative technologies in human movement science.

1.1 Contribution to Apollux Validation Study

During my research period at the Motion Analysis Lab (MAL) at Spaulding Rehabilitation Hospital, I actively contributed to a parallel project focused on validating the joint angle estimation pipeline of *Apollux*, a novel wearable sensing system designed to enable out-of-lab monitoring of human motion. The overarching objective of the Apollux project is to develop a lightweight, cost-effective solution capable of providing accurate biomechanical information by integrating kinematic and muscular data through custom-designed inertial sensors.

The aim of the study was to evaluate the accuracy of Apollux-derived joint angles for the elbow and knee during locomotor and upper-limb tasks in healthy adults. To do so, the Apollux system was tested alongside two reference platforms: the **Vicon motion capture system** (the gold standard in 3D kinematic analysis) and the **Xsens Awinda system**, a commercial wearable IMU-based solution. These systems were used concurrently to benchmark Apollux joint angle estimations.

Experimental Setup and Data Collection

I was responsible for the execution of experimental sessions, managing every aspect from system preparation to data acquisition. Each participant was equipped with:

- Reflective markers placed on anatomical landmarks (e.g., pelvis, thigh, shank, arm, forearm) for Vicon tracking.
- Xsens Awinda IMUs securely mounted on the same segments.
- Apollux IMU-based devices, fixed with adhesive tape and straps to prevent motion artifacts.

Participants performed two types of tasks:

1. **Walking trials** along a 12-meter instrumented walkway at a self-selected pace.
2. **Hand-reaching trials** to assess upper-limb motion.

Each session was conducted under my supervision, ensuring that all three systems recorded synchronized data throughout the trials.

Data Extraction and Processing
After data acquisition, I handled the entire pre-processing workflow for all systems:

- **Vicon:** Marker labeling, trajectory filtering, gap filling, and segment orientation reconstruction using Nexus.
- **Xsens:** Extraction of joint angle and orientation data via MVN Analyze.
- **Apollux:** Parsing and pre-processing of raw accelerometer and gyroscope data logged by the custom hardware.

Data Synchronization
Given the asynchronous nature of the three systems, precise temporal alignment was essential. I developed custom MATLAB scripts to:

- Extract and parse timestamps from Vicon and Apollux logs.
- Identify shared reference events (e.g., still postures or foot strikes) for initial alignment.
- Apply interpolation and offset correction for precise signal alignment across systems.

These scripts enabled frame-level alignment of the joint kinematic data and allowed for consistent comparison between platforms.

Code Development and Documentation
To facilitate reproducibility, I developed a structured and well-documented codebase capable of automating the extraction, synchronization, and processing of data across multiple trials and subjects. This pipeline significantly accelerated the processing and minimized human error in data handling.

Summary
This project provided an opportunity to strengthen my practical skills in experimental

biomechanics, multi-platform motion capture, and sensor fusion. My contributions ensured datasets that are currently being used to validate the Apollux joint angle estimation pipeline. The experience also deepened my understanding of inertial sensor integration, real-time data processing, and algorithmic validation in the context of wearable biomechanics research.

Chapter 2

Introduction

Anatomically positioned at the back of the lower leg, the Achilles tendon is the largest and strongest tendon in the human body. It connects the triceps surae muscle group - comprising the gastrocnemius and soleus - to the calcaneus (heel bone). Contraction of these muscles transmits force through the tendon, producing foot plantarflexion. This musculotendinous unit plays a vital role in locomotion and propulsion during walking, running, and jumping, enduring some of the highest mechanical loads in the human body [1]. Despite its strength, the AT is highly prone to injury, particularly in physically active men aged 30–50 [2].

Traditional rehabilitation often involves ankle immobilization, which offers protection but may lead to muscle atrophy, thrombotic risk, and impaired tendon function. Active AFOs present a promising alternative by providing controlled mobility that supports functional movement, reduces pain, and lowers re-injury risk. Powered AFOs, in particular, can assist gait by offloading the triceps surae, thereby decreasing AT loading.

The following section outlines the anatomical and physiological characteristics of the AT, current clinical management strategies, and available rehabilitation approaches. It also introduces the musculoskeletal modeling platforms used in this study to simulate movement and assess human-robot interaction, laying the groundwork for the analyses presented.

2.1 Achilles Tendon Overview

2.1.1 Anatomy, Function, and Injuries

The Achilles tendon (AT) is the largest and strongest tendon in the human body, connecting the gastrocnemius and soleus muscles (triceps surae) to the calcaneus [3]. It spans the knee, ankle, and subtalar joints and plays a central role in plantarflexion during push-off in gait [3]. Structurally, the AT consists mainly of type I collagen and features a spiral architecture with a medial rotation of 11 to 90 degrees, enhancing energy storage and mechanical efficiency while rendering the mid-portion (*watershed area*) more vulnerable to poor vascularization and rupture [4].

Functionally, the AT stores elastic energy during mid-stance via eccentric contraction of the triceps surae and releases it during push-off, improving locomotor efficiency [5, 6]. Its high stiffness supports effective force transmission and lowers the metabolic cost of walking and running.

Despite its strength, the AT is susceptible to injuries, that often result from sudden plantarflexion, overuse, or degenerative changes, and are frequently misdiagnosed. Long-term effects include tendon elongation, reduced stiffness, and impaired function, which can significantly hinder mobility and performance [3, 7].

Both operative and nonoperative treatments are effective for managing ruptures. Postoperative strategies have shifted from prolonged immobilization toward early functional rehabilitation, with modern orthotic designs enabling immediate weightbearing and improved recovery [8].

2.1.2 Passive and Active Ankle-Foot Orthoses in Achilles Tendon Rehabilitation

Ankle-foot orthoses (AFOs) affect plantar flexor activation during walking and are increasingly used to reduce muscle and tendon loading during rehabilitation. However, the intensity and timing of the external torque they apply can influence neuromuscular coordination and muscle–tendon dynamics, underscoring the need for careful design and control [9].

Passive AFOs generate torque through their mechanical properties, primarily stiffness and equilibrium angle, which define resistance to ankle dorsiflexion and plantarflexion. They help limit joint motion, stabilize the ankle, and facilitate early gait retraining, while potentially lowering metabolic cost [10]. In AT rehabilitation, passive AFOs support early weight-bearing and help prevent reinjury [11]. However, their biomechanical impact on the muscle–tendon unit (MTU) is not fully understood, and their inability to actively generate torque limits their adaptability to individual needs [12].

Active (powered) AFOs use actuators to provide adjustable torque in both magnitude and timing [9]. They are particularly effective during push-off, when AT loading peaks, by reducing plantar flexor activation and unloading the tendon [13]. Their programmability allows for subject-specific assistance across rehabilitation phases. However, their added mass and mechanical complexity may increase metabolic cost and require more refined biomechanical integration [9].

A deeper understanding of how active AFOs affect AT loading and MTU dynamics is essential to inform the design of effective, evidence-based rehabilitation strategies.

2.2 Non-invasive estimation of Achilles Tendon Unloading

Although joint kinematics, ground reaction forces, and muscle activity can be measured non-invasively using motion capture systems, force plates, and electromyography,

quantifying internal structures such as muscle-tendon forces and joint contact loads remains a significant challenge [14]. Direct in vivo measurements of tendon loading are invasive and not feasible in most research settings, suggesting the development of indirect, non-invasive techniques to estimate AT force.

Among these, ultrasound imaging has proven to be a powerful tool to evaluate tendon elongation and estimate force when combined with tendon stiffness. Accuracy improves with a subject-specific measure of stiffness and when the relative activation of the triceps surae muscles is taken into account through EMG data. Dick et al. [15] demonstrated that ankle moments derived from ultrasound-based tendon strain match inverse dynamics estimates within approximately 10%. However, the method's sensitivity to the tendon slack length that is assumed and non-uniform strain distribution is a source of ongoing limitations.

Another promising technique is shear wave tensiometry, which estimates tendon stress based on wave propagation speed. Keuler et al. [16] validated this method by calibrating it against isometric contractions, finding a strong correlation (R^2 ~0.90) between squared wave speed and tendon stress. This approach has the advantage of capturing loading dynamics during gait phases, such as late swing, that are difficult to evaluate with inverse dynamics. Nevertheless, the method requires subject-specific calibration, which may be problematic in pathological populations, and relies on assumptions regarding tissue density and wave propagation mechanics.

Bolus et al. [17] introduced an alternative wearable approach using burst vibrations from a skin-mounted actuator and accelerometer. Their system quantifies the tendon's transient mechanical response and infers load through machine learning. With R^2 values around 0.85 for ankle moment prediction, it shows potential for real-time AT monitoring. However, sensor placement sensitivity, the absence of a standard calibration protocol, and technological readiness for clinical deployment remain critical limitations.

In summary, although non-invasive methods for estimating AT load are advancing rapidly, each comes with limitations imposed by accuracy, complexity or applicability. Ultrasound and shear wave methods provide physiologically interesting data but require calibration and specialized equipment. Vibration-based systems show promise wearable-oriented solution, but need further validation. These constraints underscore the need for complementary strategies that can bridge the gap between laboratory-based accuracy and outside-world feasibility.

2.2.1 Musculoskeletal Simulations to Study Achilles Tendon Load

To address the limitations of experimental techniques, musculoskeletal (MSK) modeling has gained traction as a powerful, non-invasive approach for estimating internal biomechanical quantities such as muscle and tendon forces. MSK simulations integrate motion capture, ground reaction forces, and anatomical models to estimate how muscles coordinate movement and load tendons throughout dynamic tasks [18].

MSK simulations provide a non-invasive alternative, enabling the estimation of

internal quantities such as muscle and tendon forces. Although promising, subject-specific models for studying AT load after tendon rupture and repair remain limited [19].

By modeling muscle coordination during gait, MSK simulations offer insight into how plantar flexors contribute to propulsion and tendon loading, especially during push-off. This is essential for assessing the biomechanical impact of interventions such as ankle-foot orthoses.

In this study, we employ two platforms - OpenSim and MyoSuite - to estimate AT forces during walking under varying assistance conditions, aiming to improve our understanding of tendon loading and recovery.

Opensim

OpenSim is a widely used open-source platform for modeling, simulating, and analyzing the neuromusculoskeletal system [20]. It enables the construction of detailed biomechanical models that incorporate bones, joints, muscles, and physiological dynamics such as muscle–tendon interactions and joint constraints.

A major advantage of OpenSim is its ability to generate subject-specific models, allowing simulations to be tailored to individual anatomy and clinical conditions [21]. This makes it particularly useful in rehabilitation research, where it can be used to study the biomechanical impact of injuries, surgeries, and assistive devices.

OpenSim's muscle models are based on decades of experimental research and have been adapted for human movement analysis. The platform includes computational tools for inverse kinematics, inverse dynamics, static optimization, and forward simulations, enabling the estimation of muscle forces, joint moments, and tendon loads. It is especially effective for analyzing lower-limb function during gait and has been extensively applied in clinical and performance-related studies.

MyoSuite

MyoSuite is a simulation framework that integrates physiologically accurate musculoskeletal modeling with reinforcement learning and control algorithms [22]. Built on the MuJoCo physics engine, it enables real-time simulation of muscle-driven movements, including complex, contact-rich tasks [23]. Compared to traditional biomechanical platforms, MyoSuite prioritizes computational speed, modularity, and compatibility with machine learning, making it ideal for exploring adaptive motor control and personalized assistance strategies.

MyoSuite models are derived from OpenSim models and converted using a dedicated pipeline called MyoSim [23], which includes:

- **Geometry transfer**: maps segment geometries, muscle attachment points, and wrapping surfaces.
- **Moment arm optimization**: adjusts 3D positions of wrapping sites to match realistic moment arms.

- **Muscle force optimization**: tunes muscle parameters to replicate biomechanical behavior in MuJoCo.

By simulating neuromuscular control under various conditions, MyoSuite provides a powerful tool for investigating muscle coordination, tendon loading, and subject-specific interventions. Although still under active development, it complements platforms like OpenSim by offering faster, more flexible simulations suited for learning-based approaches and real-time applications.

2.3 Objectives of the Manuscript

This study has two main objectives, both clinical and methodological. The first objective of this study is to evaluate the impact of active AFOs on muscle activation patterns and Achilles tendon (AT) loading. We tested three levels of torque assistance - low, medium, and high - applied bilaterally by Dephy ExoBoots (Dephy, Inc. [24]) worn by healthy participants walking on an instrumented treadmill. Surface electromyography (sEMG) signals were recorded from the triceps surae and Tibialis Anterior muscles to examine changes in muscle activation across conditions. Specifically, we hypothesized:

- a reduction in triceps surae muscle activity with increasing levels of external torque;
- a stable activation pattern in the Tibialis Anterior, indicating that the AFO assistance does not interfere with normal dorsiflexor function.

To estimate Achilles tendon loading, we conducted both EMG-informed and non-informed forward dynamic simulations using OpenSim (v4.4) and MyoSuite. These simulations reproduced lower-limb motion and generated muscle–tendon dynamics across assistance levels. The activations of the Soleus, Gastrocnemius (Medialis and Lateralis), and Tibialis Anterior were used to assess the extent to which external torque reduced muscle demand and tendon force.

The second objective of this work was to compare the outcomes of two musculoskeletal simulation platforms - OpenSim and MyoSuite - in estimating AT loading, from inverse kinematics to muscle force generation under assisted walking conditions. This comparison aims to identify the strengths, limitations, and consistency of each tool in the context of human–robot interaction and rehabilitation research.

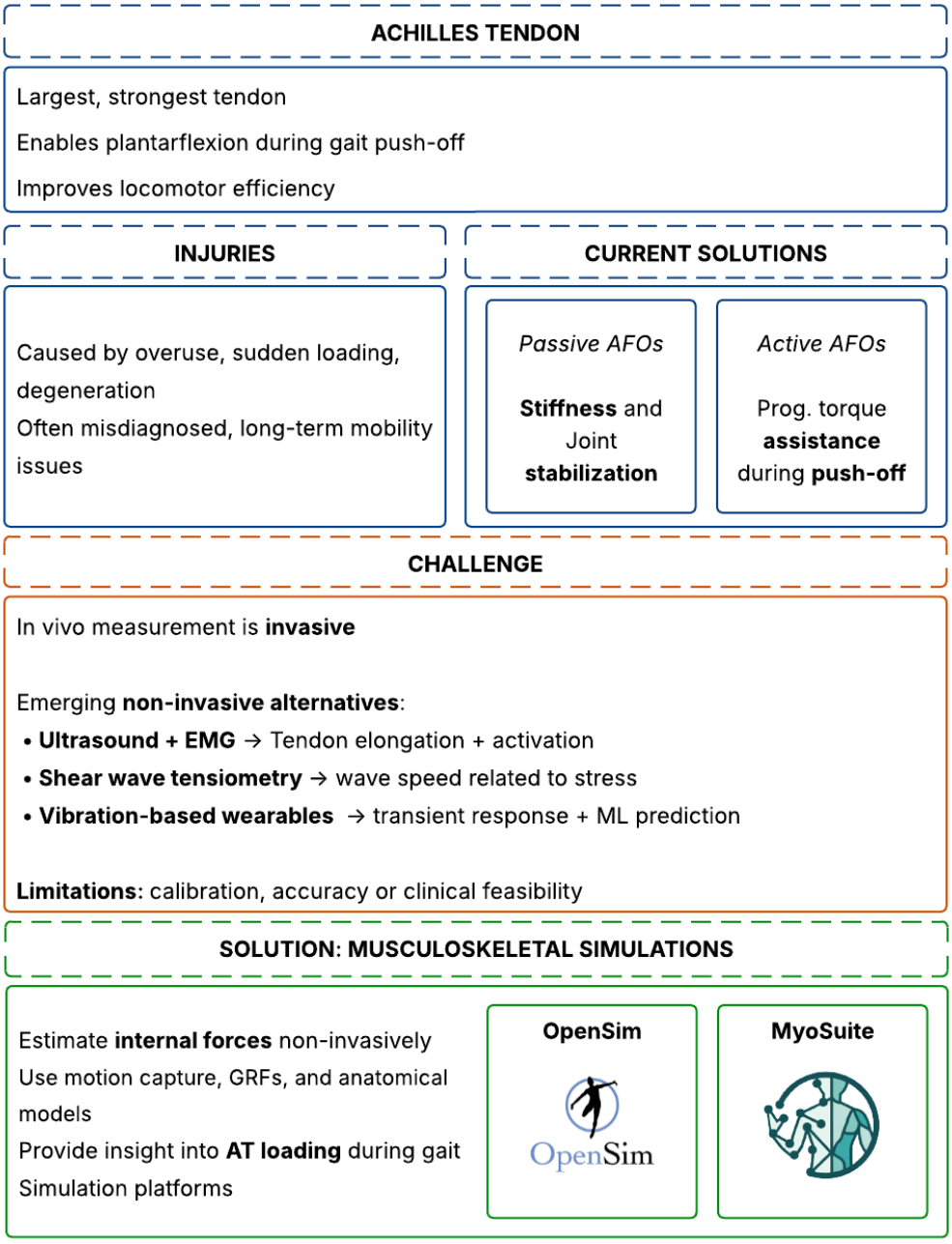

Figure 2.1: Conceptual flow of the study rationale. Overview of the Achilles tendon's biomechanical function, common injury mechanisms, and current rehabilitation strategies using passive and active ankle-foot orthoses (AFOs). Due to the invasiveness of direct tendon load measurements, emerging non-invasive techniques are explored, though each has notable limitations. Musculoskeletal simulations offer complementary solutions to estimate internal tendon loading during gait, with OpenSim and MyoSuite providing two distinct modeling platforms used in this study.

Chapter 3

Materials

3.1 Participants

Data were collected from 11 healthy participants (5 female, 24.4 ± 1.7 years), recruited from Spaulding Rehabilitation Hospital in Charlestown, MA. The average body weight was 71 ± 8kg. All participants met the inclusion criteria: they were free from medical conditions that could affect lower-limb movement or compromise safety during study procedures, and had no skin lesions, infections, or rashes in areas where motion capture markers would be placed. Prior to participation, each subject underwent screening and was thoroughly informed about the study objectives, procedures, potential risks, and benefits. Written informed consent was obtained from all participants. The study was approved by the Institutional Review Board (IRB) at Spaulding Rehabilitation Hospital (protocol #2024P000655).

Table 3.1: Anthropometric data of study participants.

Code	Height (m)	Weight (kg)
P00	1.96	86.02
P01	1.74	63.04
P02	1.70	70.84
P03	1.63	60.34
P04	1.75	71.86
P05	1.89	81.60
P06	1.66	66.97
P07	1.64	71.76
P08	1.78	65.25
S05	1.85	81.60
S06	1.80	67.50

3.2 Study procedure

3.2.1 Preliminary steps

All experimental procedures were performed at the Spaulding National Running Center (SNRC), located within the Spaulding Hospital Cambridge (SHC). Each participant completed a single study visit lasting approximately 3.5 hours.

Prior to the visit, a brief screening questionnaire was administered to determine eligibility. Eligible individuals were invited to participate and instructed to wear comfortable clothing on the day of testing.

Upon arrival, participants were guided through the informed consent process, which was conducted by a trained member of the research team with appropriate academic or professional credentials, as designated by the Principal Investigator. Once consent was obtained, demographic data (e.g., age, gender) and anthropometric measurements were collected using standard tools. These included height, weight, limb segment lengths, joint widths, and limb circumferences, necessary for personalized biomechanical modeling.

Participants were then prepared for data collection. Reflective markers and surface EMG electrodes were applied according to standard procedures, with appropriate skin preparation to ensure signal quality. Electrodes targeted key lower limb muscles (gastrocnemius lateralis/medialis, soleus, tibialis anterior) and were secured with adhesive and wrap. Additionally, smartphone video recordings were acquired using the MyoLab app (MyoLab, USA) for qualitative assessment and calibration.

3.2.2 Instrumentation

Vicon motion capture system

The Vicon Motion Capture System (Vicon, Oxford, UK) is a high-precision optical tracking technology widely used in biomechanics and clinical research, and is considered the gold standard for human movement analysis [25]. It employs an array of infrared cameras to track the three-dimensional positions of retroreflective markers placed on anatomical landmarks across the body. Using triangulation, the system determines marker trajectories with sub-millimeter accuracy within a calibrated laboratory space.

As illustrated in Figure 3.1, the laboratory setup included ten high-resolution infrared cameras and two standard RGB cameras, all operating at a frame rate of 250 Hz. The RGB cameras, along with smartphone video recordings, were positioned at the back and left sides of the capture volume. These additional recordings provided complementary visual perspectives, particularly focused on the lower limbs, to assist with qualitative analysis and facilitate system calibration.

To enable replication of full-body motion within musculoskeletal (MSK) modeling software, we aimed to acquire accurate kinematic data during both unassisted and assisted walking trials. Motion capture was performed using 53 reflective markers

strategically placed across the body. These included both anatomical markers, positioned over key joint landmarks for precise biomechanical analysis, and tracking markers used to support segment orientation.

Figure 3.1: Spaulding National Running Center, located within Spaulding Hospital Cambridge. Ten high-resolution infrared cameras, two standard RGB cameras and AMTI instrumented treadmill.

For upper body and trunk motion, we adopted the Plug-In Gait Full-Body marker set [26], while lower limb kinematics were captured using the IOR Gait Full-Body model [27], as illustrated in Figures 3.2 and 3.3. In situations where the Dephy ExoBoot interfered with direct marker placement on the knee and ankle (e.g., due to mechanical obstruction), we replaced anatomical markers with clusters of four tracking markers on each thigh and shank to ensure reliable segment tracking.

To maintain marker stability and reduce the risk of detachment during walking, all markers were secured using double-sided tape and reinforced with adhesive material when necessary. In Figure 3.2, an example of marker placement on the body of a subject during data collection is shown.

Surface Electromyography Acquisition with the Delsys System

To assess muscle activation during gait, we employed the *Delsys Trigno System* (Delsys Inc., Natick, MA, USA) for wireless surface electromyography (sEMG) data acquisition. This system is widely recognized for its high signal fidelity and low noise interference, making it ideal for biomechanical and neuromuscular analysis during dynamic tasks.

sEMG signals were recorded from eight muscles, four per lower limb, focusing on those primarily involved in plantarflexion and linked to Achilles tendon loading. This selection aligns with the main objective of evaluating tendon unloading across varying levels of external torque. Additionally, we included one key dorsiflexor muscle to verify that the exoskeleton assistance did not disrupt normal activation patterns

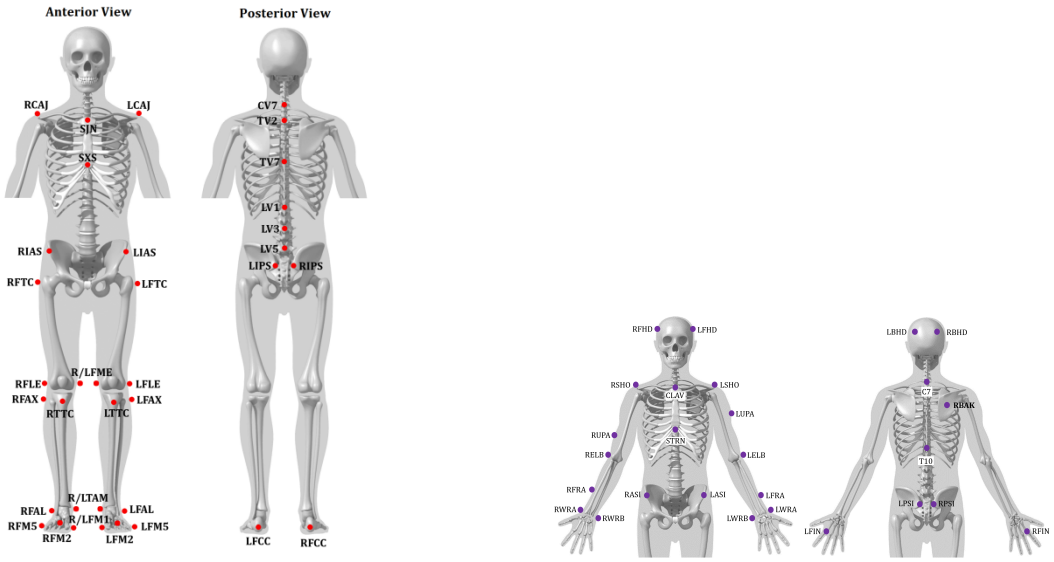

(a) (b)

Figure 3.2: (a) IOR Gait Full-Body model (Lower body). (b) Plug-in Gait upper body model.

Figure 3.3: Example of marker placement on a subject during motion capture data acquisition. Reflective markers were positioned according to the full-body protocol to track the three-dimensional motion of body segments during walking.

during gait.
The muscles monitored (see Figure 3.4) included:

- **Soleus**: A uniarticular muscle in the posterior lower leg, fundamental for maintaining posture and producing plantarflexion during the push-off phase of gait.
- **Gastrocnemius Medialis and Lateralis**: Biarticular muscles crossing both the knee and ankle joints, involved in knee flexion and ankle plantarflexion, essential for propulsion.
- **Tibialis Anterior**: Located in the anterior compartment of the lower leg, it plays a crucial role in dorsiflexion and foot clearance during the swing phase.

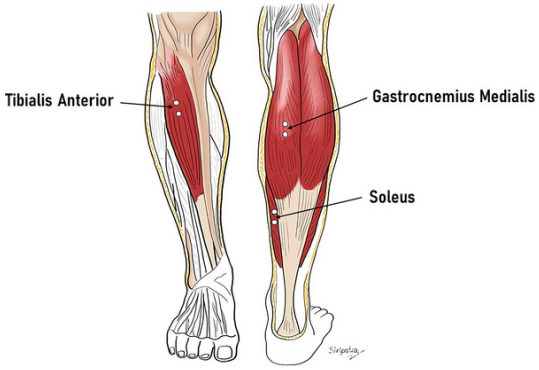

Figure 3.4: Muscles considered for the ankle joint analysis: gastrocnemius medialis, gastrocnemius lateralis, and soleus (plantarflexors), and tibialis anterior (dorsiflexor).

Before electrode placement, the skin was cleansed using isopropyl alcohol to remove surface contaminants and ensure good electrical contact. Sensors were positioned over the midline of each muscle belly, aligned with the muscle fiber orientation, using the Delsys Adhesive Sensor Interface [28]. This alignment ensures that the parallel bar detection surfaces accurately capture electrical activity along the direction of propagation.

To validate sensor positioning, subjects performed brief isometric contractions of each target muscle. Electrode placement was adjusted as needed to maximize signal amplitude and reduce cross-talk. Once optimized, electrodes were further secured with medical-grade tape to minimize motion artifacts during data collection.

Figure 3.5 illustrates the anterior and posterior electrode configurations used during testing.

Instrumented Treadmill

To collect kinetic data during walking trials, we used an *AMTI tandem instrumented treadmill* (AMTI, Watertown, MA, USA) equipped with two six-axis force platforms embedded beneath each treadmill belt. The treadmill features a compact, front-to-back *split-belt design*, which avoids limitations associated with traditional side-by-side

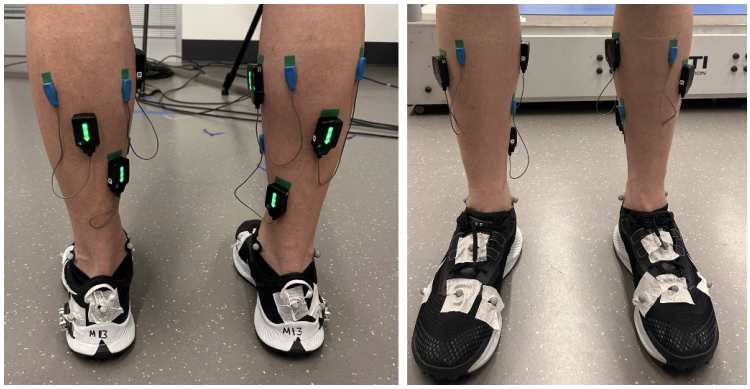

Figure 3.5: EMG placement on lower limbs, targeting plantaflexor muscles of the triceps surae and tibialis anterior (dorsiflexor).

configurations. This setup allows for the independent measurement of ground reaction forces (GRFs) from each limb, including during the double-support phase of gait.

Each force plate captures three-dimensional force components—**vertical**, **anterior-posterior**, and **medial-lateral**—as well as **moments** about the sagittal (flexion-extension), frontal (abduction-adduction), and transverse (internal-external) axes. These measurements are critical for evaluating external loads acting on the body during locomotion.

The treadmill system was connected to a data acquisition unit, and the force signals were processed using *Visual3D* (C-Motion, Inc.), that enables synchronized integration of kinetic and kinematic data, allowing for the estimation of joint forces and torques through inverse dynamics.

The treadmill was installed at the Spaulding Running Center Laboratory in Cambridge, MA, and configured to facilitate both unassisted and assisted walking trials.

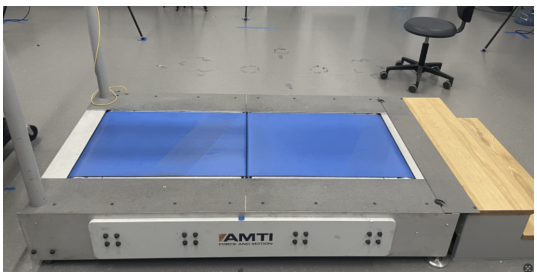

Figure 3.6: AMTI Tandem Instrumented Treadmill used at the Spaulding Running Center Laboratory (Cambridge, MA).

Active Dephy ExoBoot

As discussed previously, active ankle-foot orthoses (AFOs) offer significant advantages for rehabilitation by not only providing mechanical support and stability, but also actively assisting movement. Unlike passive devices that limit joint motion, active AFOs apply controlled torques to promote functional muscle use, facilitate weight-

bearing activities, and enable progressive motor recovery while minimizing the risk of re-injury.

In this context, *Dephy Inc.* (Maynard, MA, USA) developed the **ExoBoot EB60**, a lightweight, wearable robotic AFO designed to provide assistive torque at the ankle joint. The ExoBoot delivers external torque during *plantarflexion*, targeting the stance phase of gait when activation of the triceps surae muscles and consequently loading of the Achilles tendon is at its peak. The device is illustrated in Figure 3.7.

Figure 3.7: Active Dephy ExoBoot (EB60) by Dephy Inc. [24].

The ExoBoot system includes actuators mounted on the shanks and rigid braces attached to the shoes, with each unit weighing approximately **1.2 kg**. Participants wore a pair of ExoBoots bilaterally to promote symmetrical gait patterns and natural loading conditions across limbs. During data collection, both unassisted and assisted walking trials were performed, structured into five conditions based on the level of device engagement.

To modulate the assistance provided, we adjusted a device-specific parameter called the *Augmentation Level*, which controls the magnitude of the torque applied at the ankle during gait. This setup enabled a systematic investigation of the ExoBoot's effects across varying support levels.

The experimental design aimed to evaluate the device's capacity to influence lower-limb muscle recruitment and modulate Achilles tendon loading. By analyzing both EMG and biomechanical data under different augmentation levels, we assessed the ExoBoot's potential as a tool for functional rehabilitation and performance support.

3.2.3 Softwares

Six primary software tools were employed to carry out the data processing and analysis for this study:

- **OpenSim** (version 4.4, Delp et al., 2007) [29]: Used for generating subject-specific musculoskeletal simulations, OpenSim played a central role in estimating muscle activations and Achilles tendon forces. The software enabled the construction of personalized models and the execution of inverse kinematics (IK), Reisdual Reduction Algorithm (RRA), and Computed Muscle Control (CMC) to investigate biomechanical aspects of assisted and unassisted walking.

- **Vicon Nexus** (version 2.15, Oxford Metrics, UK): This software was responsible for acquiring and labeling both kinematic and surface electromyography (sEMG) data. Nexus served as the initial interface for motion capture, managing data collection and marker tracking from the Vicon system.

- **Visual3D** (C-Motion Inc.) [30]: Visual3D was used to compute and extract kinematic and kinetic data, including ground reaction forces (GRFs), joint angles and joint torques. Static calibration trials and dynamic gait trials exported from Vicon Nexus were processed in Visual3D to generate GRF and IK outputs, which were later exported for downstream analyses.

- **MyoLab App** [23]: An early-stage smartphone application developed within the MyoSuite ecosystem, MyoLab was used to record RGB video data from range-of-motion (ROM) tasks. The app collects metadata (e.g., body mass, subject ID) and captures full-body motion to support the creation of subject-specific digital twins for future simulation and analysis.

- **MyoSuite Executables**: A suite of command-line tools developed in the MyoSuite pipeline [23], including:

  - `embeddedIK.exe` – for performing inverse kinematics on motion capture trials.
  - `estimateATF.exe` – for estimating Achilles tendon force using forward dynamics simulations.
  - `getMarkerErrors.exe` – to quantify residual marker errors during IK fitting.
  - `moveMarkerSet.exe` – for marker set transformation and model alignment.

  These executables enabled automated batch processing of IK and ATF estimations across trials and subjects, contributing to an efficient and reproducible simulation workflow.

Together, these software platforms enabled a comprehensive pipeline for capturing, processing, and analyzing experimental and simulated biomechanical data. The integration of motion capture, musculoskeletal modeling, and data-driven tools facilitated a detailed investigation into muscle coordination and Achilles tendon unloading across different assistance conditions.

3.2.4 Experimental procedure

Each experimental session was structured into a sequence of standardized steps to ensure consistency and high-quality biomechanical data acquisition. The protocol combined full-body motion capture, electromyographic recordings, and wearable robotics testing, across multiple walking and calibration conditions.

Preparation and Setup

Before initiating data collection, all equipment was tested to confirm proper recording functionality. Participants were prepared by applying 53 reflective markers and eight sEMG electrodes, as previously described. The Delsys EMG system was synchronized with the Vicon Nexus platform by naming each electrode and linking muscle channels in the software configuration.

Vicon System Calibration: The laboratory was first cleared of reflective objects, and the Vicon camera system was calibrated using a wand emitting infrared light. The global coordinate system was then defined using the Vicon calibration plugin, centering the volume around the instrumented treadmill. This ensured spatial accuracy for the 3D motion capture.

MVC Recordings: Maximum voluntary contractions (MVCs) were recorded for each monitored muscle to normalize the sEMG signals across subjects and walking conditions.

Baseline Trials

Static Trial Without Device: A baseline static trial was conducted with participants standing upright (arms extended, feet shoulder-width apart) to capture anatomical landmarks and body mass distribution without the ExoBoots. This served to scale the musculoskeletal model and calibrate marker positions.

Range of Motion (ROM) Assessment: Participants completed isolated joint movements (15 seconds per trial) to assess ROM in the neck, shoulders, elbows, wrists, hips, knees, ankles, and spine. Each joint was tested across specific planes (flexion/extension, abduction/adduction, inversion/eversion) to support model scaling and digital twin development.

Balance and CoM Tasks: Participants performed:

- Standing
- Seated
- Single-leg balance
- Squats
- Weight shifting

These tasks evaluated postural control and provided additional input for dynamic modeling.

Unassisted Walking Trial: Participants walked at 3 and 3.3 mph (1.34 and 1.47 m/s) on the instrumented treadmill for 1.5 minutes per speed. This trial served as the control condition, capturing natural gait and muscle activation without device interference.

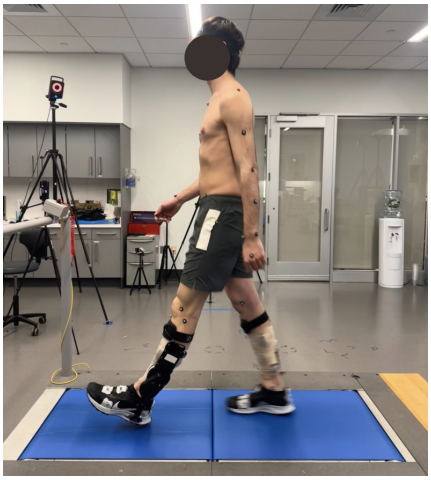

Figure 3.8: Example of a walking trial performed with the Dephy ExoBoot during the experimental data collection.

ExoBoot Trials

Second Static Trial (with ExoBoot): A second static trial was collected after fitting the bilateral Dephy ExoBoots to account for weight redistribution and altered ankle alignment.

Unpowered Walking Trial: With the ExoBoots worn but turned off, participants repeated treadmill walking at the same speeds. This allowed the isolation of mechanical effects due to device mass from the effects of active torque assistance.

System Synchronization: Prior to the powered trials, study stuff performed three rapid shaking motions of the ExoBoots while recording with both Vicon and the Dephy software. This enabled time alignment between external torque data, kinematics, and sEMG signals.

Assisted Walking Trials: With the ExoBoot activated, participants completed trials at three augmentation levels (50, 100, 150) for both speeds. After each level adjustment, a 5 minute acclimatization period allowed the device to stabilize. Data collection resumed once participants maintained a steady gait rhythm. Each trial lasted 1.5 minutes or until 30 full gait cycles were recorded.

Final Synchronization: The session concluded with a second set of three shaking motions to finalize synchronization across all recorded data streams.

This comprehensive protocol ensured the capture of high-resolution, multimodal data under both unassisted and assisted walking conditions, forming the basis for downstream musculoskeletal simulation and Achilles tendon force estimation. Figure 3.8 shows an example of a walking trial performed with the Dephy ExoBoot.

Chapter 4

Methods

4.1 Processing of Kinematics in Vicon Nexus 2.16 and Gait Cycle Segmentation

For each study participant, trajectories from 53 reflective markers were collected to reconstruct full-body kinematics using the Vicon motion capture system. Marker trajectories were processed using Vicon Nexus 2.16.

Labeling Skeleton and Model Calibration

The first step in the pipeline involved defining a labeled skeleton template using the Labeling Template Builder in Nexus. Markers were assigned to anatomical segments based on the IOR Full-Body model for the lower limbs and the Plug-in Gait model for the upper limbs. Anthropometric data, including body height, weight, leg lengths, and joint widths (knee and ankle), were entered to estimate joint center locations. An example of the static calibration trial and the resulting skeletal model reconstruction is shown in Figure 4.1. A static calibration trial was performed with the subject in an A-pose, standing on the treadmill. During this step, each marker was manually labeled to match the template structure. Two models were created for each participant: one for unassisted walking trials and one for trials with the ExoBoots, accounting for the added device weight.

Subsequently, the **Plug-in Gait Static** and **Static Subject Calibration** pipelines were run to finalize model scaling and segment alignment.

Dynamic Trial Processing

The **Reconstruct and Label** pipeline was used to assign marker trajectories to the model in dynamic trials. Although the pipeline automatically labels markers, it may not resolve brief gaps when markers disappear from view (i.e., when not seen by at least three cameras). Manual gap filling was therefore applied as needed:

- **Spline Fill**: Used for short gaps by interpolating trajectories with spline curves.

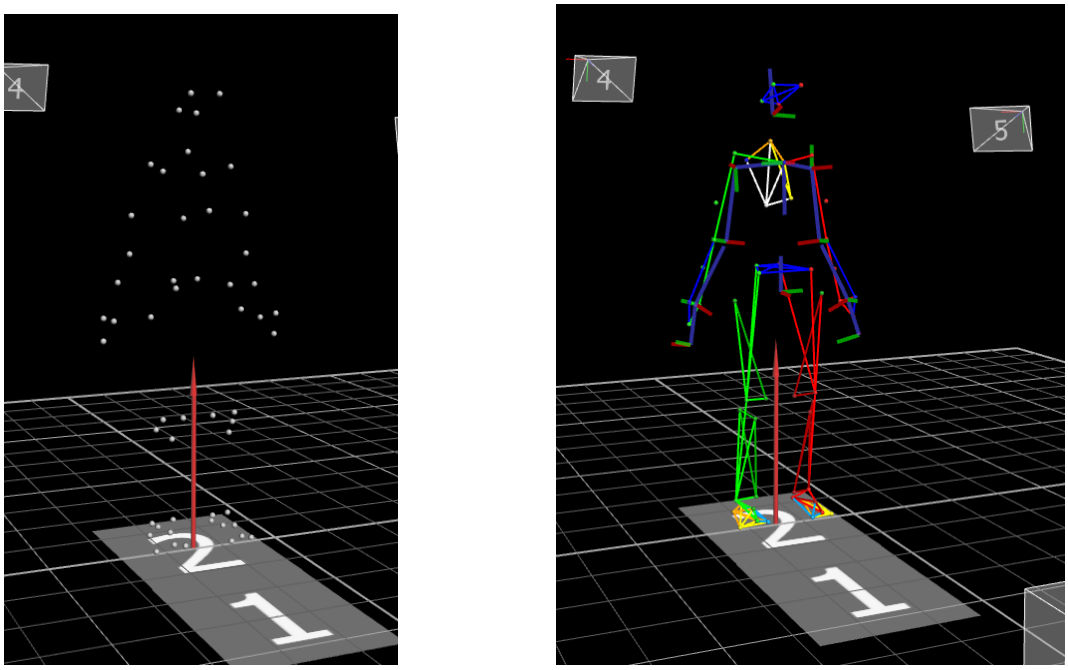

(a) (b)

Figure 4.1: Example of static calibration trial. (a) Marker set applied on the subject during the A-pose acquisition. (b) Skeletal model reconstruction generated after marker labeling, showing the segment definitions based on the IOR Full-Body and Plug-in Gait models.

- **Rigid Body Fill**: Applied when three or more rigidly connected markers were available to estimate the missing marker.
- **Pattern Fill**: Employed for repetitive movements based on cyclic patterns.

After verification of marker labeling accuracy, the dynamic processing pipeline was executed. This included filtering trajectories using a Woltring filter, computing upper joint kinematics (Plug-in Gait Dynamic Model), and exporting the processed trial as a `.c3d` file.

Gait Cycle Segmentation

Gait events were identified using the AMTI Treadmill Gait Cycle Events pipeline, which is designed for the lab's specific treadmill configuration. The pipeline was executed via MATLAB while the trial was loaded in Vicon. It used the vertical ground reaction force (Fz) signal from each force plate to detect heel strikes and toe-offs.

Key inputs included subject name, front and back force plate names, and a threshold for force detection (set at 5% of body mass). The pipeline returned gait cycle events directly into the Vicon environment. Manual inspection ensured correct detection, especially of foot-off events which can be underestimated.

The final `.c3d` files contained all relevant analog and kinematic data (raw EMG and GRFs, marker trajectories), ready for further analysis in MATLAB, OpenSim,

or MyoSuite. An example of the gait cycle segmentation process displayed in the Vicon environment is shown in Figure 4.2.

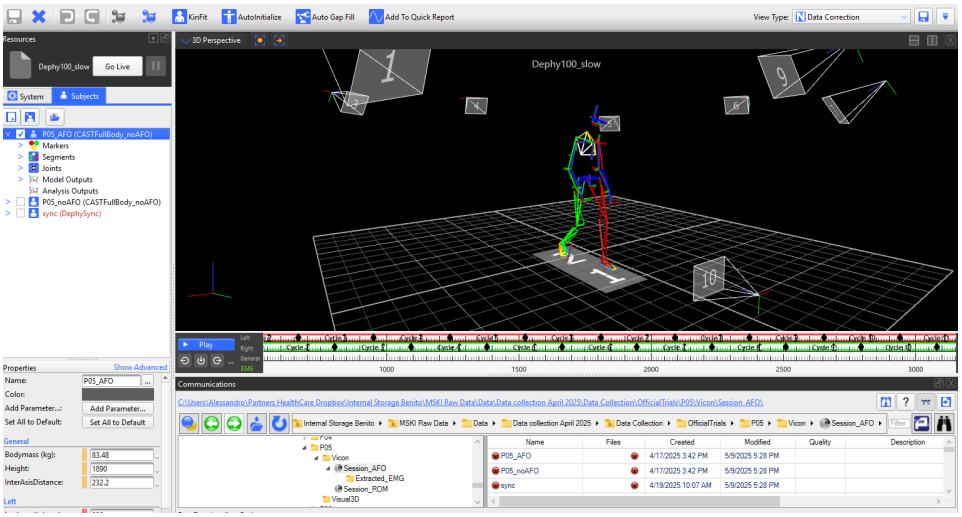

Figure 4.2: Example of gait event detection using the AMTI Treadmill Gait Cycle Events pipeline. Heel strikes and toe-offs were identified based on vertical ground reaction force signals while the trial was loaded in Vicon.

4.2 Visual3D Processing Pipeline

Visual3D (C-Motion Inc.) was used to process kinematic and kinetic data and to compute joint angles, joint moments, and ground reaction forces (GRFs). All trials were processed by importing `.c3d` files into the software and building subject-specific skeletal models.

Model Definition and Joint Configuration

For each participant, a personalized biomechanical model was constructed by combining two existing templates: the Plug-in Gait model [26] for the upper body and the IOR model [27] for the lower limbs. Anatomical marker locations and anthropometric measurements (height and weight) were used to define the geometry and inertial properties of each segment.

The upper body model included nine segments: pelvis, thorax, head, left/right upper arms, forearms, and hands. For each segment, anatomical and tracking markers were assigned, and calibration markers (e.g., medial/lateral knee) were used to define joint centers and segment orientations. The lower body model was adapted from the IOR Full-Body template to match the available marker set.

Visual3D automatically creates joints between adjacent segments when the distal end of one segment and the proximal end of another are within a defined proximity. These joints are not mechanical constraints but serve as reference points for calculating joint reaction forces and net internal moments. All joints used in this study had 6 degrees of freedom (DOF) and followed the standard segment hierarchy for gait

analysis (e.g., foot–shank–thigh–pelvis).

Once the model was defined and scaled using a static trial, it was applied to all dynamic trials. Two subject-specific models were created per participant: one for unassisted walking (body weight only) and one for assisted walking (including ExoBoot mass).

Ground Reaction Force Extraction

GRF data were extracted from trials recorded on an AMTI instrumented treadmill with two embedded force plates. Because each foot alternates contact between the two plates during walking, the system required segmenting and assigning GRF data from each plate to the corresponding foot. This was accomplished using the *Compute Model Based Data* tool in Visual3D, which assigns forces and moments to the appropriate foot segment based on contact timing and location.

Visual3D outputs included 3D force vectors and moments projected on each foot. These were visually verified within the software, with GRF projections shown as blue vectors beneath the feet. Vertical GRFs (Z-axis) were extracted and validated for each foot separately. An example of ground reaction force extraction and visualization in Visual3D is shown in Figure 4.3. Finally, GRF and moment data were exported to `.mat` format for further analysis in MATLAB. The resulting files were organized as tables with time stamps along rows and force/moment components along columns (X, Y, Z directions).

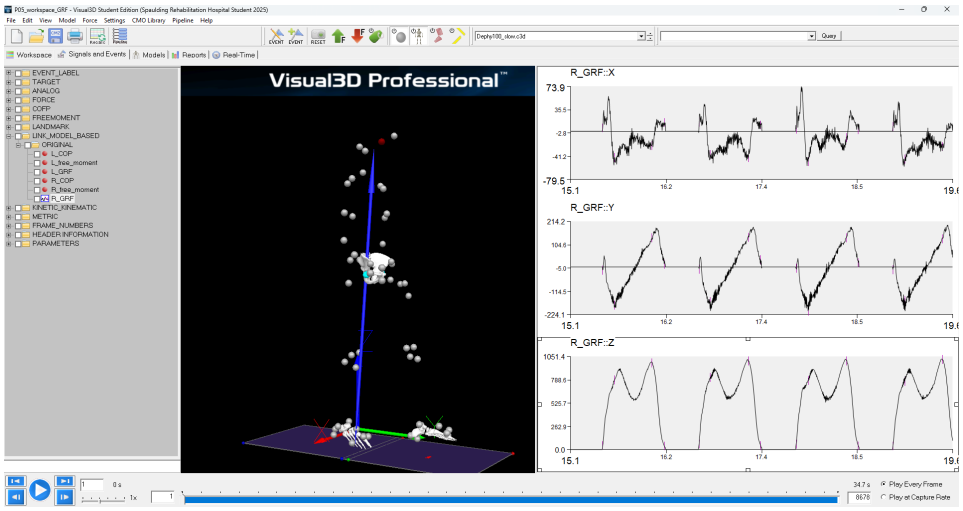

Figure 4.3: Example of ground reaction force extraction in Visual3D. Force vectors are assigned to the corresponding foot segments, with 3D forces and moments displayed alongside GRF time series in the X, Y, and Z directions.

4.2.1 Computation of Joint Angles and Torques in Visual3D

Joint angles and joint moments were computed using *Visual3D* (C-Motion Inc.), following a model-based approach grounded in rigid-body kinematics and inverse dynamics.

Joint Angle Computation

Joint angles were calculated as the relative orientation of a distal segment with respect to a proximal reference segment using a sequence of three rotational transformations (Cardan angles). For all lower limb joints, the standard **XYZ Cardan sequence** was applied, where:

- **X-axis**: Flexion/Extension
- **Y-axis**: Abduction/Adduction
- **Z-axis**: Internal/External Rotation

The coordinate system used in Visual3D assumes Z as the axial (vertical) direction and Y as the anterior–posterior (direction of progression), in line with commonly accepted biomechanical conventions [31]. No normalization was applied, meaning that joint angles were expressed directly in relation to the static calibration posture without any offset adjustment.

The following joint angles were computed for each participant:

- Right/Left Hip Angle: Thigh relative to Pelvis
- Right/Left Knee Angle: Shank relative to Thigh
- Right/Left Ankle Angle: Foot relative to Shank

The resulting signals were stored under the `LINK-MODEL-BASED` folder in Visual3D, and only the X-components (flexion/extension) were retained for further analysis.

An example of joint angle computation and visualization in Visual3D is shown in Figure 4.4.

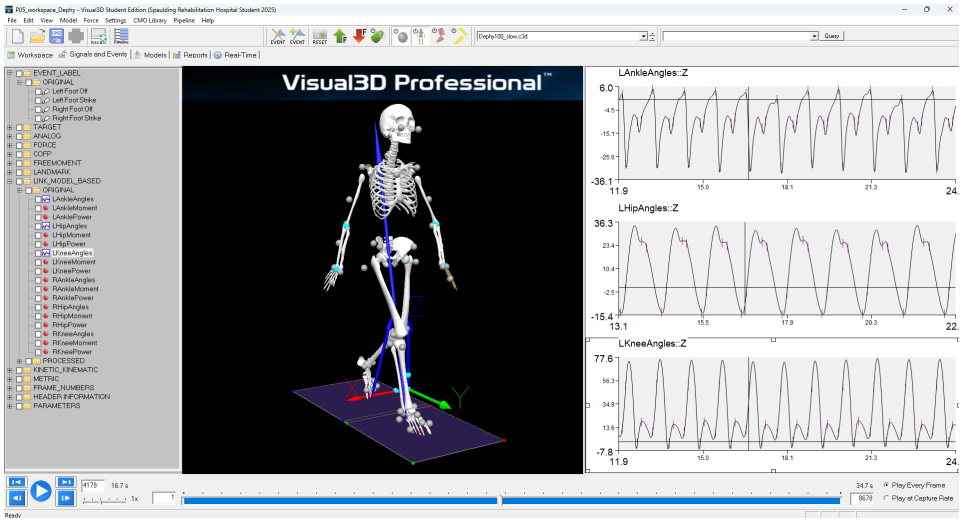

Figure 4.4: Example of joint angle computation in Visual3D. Joint angles for ankle, knee, and hip are displayed along the sagittal plane (Z-axis) over multiple gait cycles, together with the 3D model reconstruction.

Joint Moment Computation

Joint moments were computed via inverse dynamics using the same segment coordinate systems and joint definitions. Moments were resolved in the local coordinate system of the *proximal segment* (e.g., for the right knee, moments were expressed in the coordinate system of the right thigh).

Visual3D computes **net internal moments**, representing the total moment generated by muscles, ligaments, and passive structures to counteract external loads such as ground reaction forces. The sign of each component follows the **Right-Hand Rule**, meaning:

- Flexion moment about the X-axis is positive for the hip and ankle, but negative for the knee (unless negated).
- Adduction moment about the Y-axis is positive for the right leg and negative for the left leg.
- Internal rotation moment about the Z-axis is positive for the right leg and negative for the left leg.

To ensure consistent sign conventions across joints, the X-component of the knee joint moment was negated post-processing, so that flexion moments were positive across all joints.

All joint moments were normalized to subject body mass (Nm/kg) by default using Visual3D's built-in normalization tools.

4.3 Preparation of GRF and EMG data for simulation analyses

Ground Reaction Forces

Ground reaction forces (GRFs) were extracted from Visual3D and converted into OpenSim-compatible format through a three-step process:

- **Reference System Conversion**: The GRF and moment components were reordered to align with OpenSim's coordinate system, following documentation from both Visual3D and OpenSim.
- **Filtering**: A low-pass Butterworth filter was applied to remove high-frequency noise from the force and moment signals.
- **Export to .mot**: Processed data were saved in `.mot` format, compatible with OpenSim's musculoskeletal simulation tools.

This pipeline ensured consistency across trials and subjects, allowing downstream analysis of joint kinetics in OpenSim.

EMG Signal Extraction and Processing

Electromyographic (EMG) signals were acquired using the Delsys system, synchronized in real time with the Vicon Nexus system, and saved within the `.c3d` files. From each file, analog signals were extracted using the Biomechanical ToolKit (BTK) in MATLAB:

- `btkReadAcquisition`: to load the `.c3d` file
- `btkGetAnalogs`: to extract analog EMG signals

Signals were recorded at 2000 Hz for four muscles per leg: Soleus, Gastrocnemius Medialis, Gastrocnemius Lateralis, and Tibialis Anterior.

The EMG processing pipeline included the following steps:

1. **Rectification**: Absolute value of the signal to preserve activation magnitude.
2. **Band-pass filtering**: Fourth-order Butterworth filter with 10–450 Hz cutoffs.
3. **Normalization**: Each signal was normalized to the Maximum Voluntary Contraction (MVC) recorded for that muscle.

This processed and normalized EMG data was then used to assess muscle recruitment under different walking conditions and device assistance levels.

Ankle Torque Extraction from the Dephy ExoBoot

The torque profiles generated by the Dephy EB60 ExoBoot were recorded using the companion tablet application provided by the manufacturer. This app enabled configuration of device parameters, selection of assistance levels, and real-time recording of both timestamps and external torque data during walking trials.

Three distinct assistance conditions were defined: low, medium, and high, each corresponding to increasing levels of support delivered during the stance phase of the gait cycle. As the assistance setting increased, the magnitude of the applied torque also rose, particularly during the push-off phase (approximately 40–60% of the gait cycle). During swing, the device remained passive, allowing unassisted motion.

The torque signals recorded for each condition were exported directly from the app and later integrated into the OpenSim and MyoSuite simulations. These data served as the external input for the actuated ankle joint in the musculoskeletal model, enabling a direct comparison between assisted and unassisted walking biomechanics.

4.4 MyoSuite Processing Pipeline

The musculoskeletal simulation workflow developed for this study leverages the MyoSuite framework and is organized into a structured, four-stage pipeline. This pipeline transforms experimental motion capture data and ground reaction forces (GRFs) into neuromuscular simulations capable of estimating joint kinematics, muscle

activations, and Achilles tendon force (ATF) under both assisted and unassisted walking conditions. Each stage is executed using a dedicated computational tool, enabling a reproducible and scalable analysis across multiple subjects and trials. A typical example of the MyoSuite simulation environment is shown in Figure 4.5, which provides a physiologically-inspired virtual space for musculoskeletal modeling and control development [23].

Figure 4.5: Example of the MyoSuite simulation environment. MyoSuite provides a physiologically-inspired virtual platform for neuromuscular modeling and motor control development, enabling realistic simulations of musculoskeletal systems.

4.4.1 Subject Preparation and MarkerSet Definition

The process begins with subject preparation and marker set definition. For each participant, a subject-specific marker set file was manually curated and saved in XML format. This file establishes the anatomical correspondence between the experimental markers acquired via motion capture and the virtual markers placed on the musculoskeletal model. The model used in this phase is either the `myoskeleton` [32] or `myolegs` [33] variant from the MyoSuite model library, both of which are based on OpenSim and include muscle-tendon units and torque actuators.

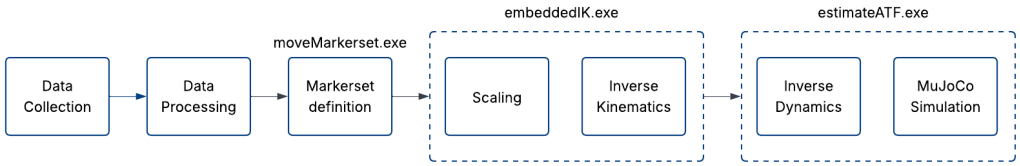

Figure 4.6: MyoSuite-based Achilles tendon force estimation pipeline. Overview of the processing steps used to estimate Achilles tendon force (ATF) using musculoskeletal simulations in MyoSuite. The pipeline includes data collection and processing, marker set adjustment (`moveMarkerset.exe`), scaling and inverse kinematics (`embeddedIK.exe`), and finally, inverse dynamics and MuJoCo-based simulations (`estimateATF.exe`).

4.4.2 Model Scaling and Inverse Kinematics (IK)

After associating the marker data with the base model, the subject's anatomy is calibrated by scaling the model dimensions to match their anthropometry. This is achieved by minimizing the distance between experimental and virtual markers in a static pose, a process implemented through the `moveMarkerSet.exe` and `getMarkerErrors.exe` executables.

Following scaling, dynamic trial data are used to compute joint kinematics through inverse kinematics using `embeddedIK.exe`. Although scaling and IK are often treated as separate steps, they form two complementary aspects of the same optimization problem, deriving joint angle trajectories from experimental marker data. For every time instant, the IK solver minimizes a cost function that adjusts the angular positions of the model to reduce the marker position error. Without accurate scaling, IK results become meaningless, and vice versa: one cannot correctly interpret joint angles unless the model has first been anatomically matched to the subject.

This process produces subject-specific joint angle trajectories and residual marker errors, both essential inputs for the subsequent stages of biomechanical simulation.

4.4.3 Inverse Dynamics and Muscle Force Estimation

The second stage focuses on inverse dynamics (ID) and muscle force estimation using a modified `myolegs` model adapted from the Rajagopal full-body model. Given the joint angles from IK, the goal of ID is to compute the net joint torques and corresponding muscle forces necessary to produce the observed motion.

This is formulated as a constrained optimization problem, where the objective is to minimize the error between the torques generated by the muscles and the torques required by the kinematic trajectories. A regularization term is included to penalize excessive muscle activation, favoring biologically plausible, energy-efficient activation strategies. This addition addresses the muscle redundancy problem, where multiple combinations of muscle activations can lead to the same joint kinematics. Among the many possible solutions, the solver selects the one that minimizes overall activation, consistent with human neuromuscular control principles.

Technically, the process begins with estimating required joint accelerations and torques using `mj_inverse`, then proceeds to solve for the muscle activations that best reproduce these torques. This approach builds upon the methodology illustrated in MyoSuite's `tutorial_6` [34], and was implemented in batch using dedicated command-line tools.

Incorporating the Dephy ExoBoot

To simulate assisted walking conditions, the model incorporates the Dephy ExoBoot as an ideal torque actuator at the ankle joints. The actuator is driven by the experimental torque profiles recorded during walking with the device, and its inertial mass is added to the tibial segments to account for its mechanical effect on limb

dynamics. This modification ensures that the simulations realistically reflect the altered loading conditions introduced by the exoskeleton.

4.4.4 Muscle Force and Activation Outputs

The final stage of the pipeline yields a comprehensive set of simulation outputs, including time-resolved profiles of muscle activations, individual muscle forces, net joint torques, and angular velocities. Among these, special focus is placed on the estimation of Achilles tendon force (ATF), which is computed as the sum of the forces produced by the soleus, gastrocnemius medialis, and gastrocnemius lateralis muscles. These muscles collectively contribute to plantarflexion torque and are primary transmitters of force through the Achilles tendon.

The tibialis anterior is also analyzed due to its antagonistic function in dorsiflexion and its critical role in ensuring appropriate foot clearance during both the swing and push-off phases of gait. Monitoring both plantarflexor and dorsiflexor activity enables a more complete understanding of neuromechanical coordination and potential compensatory strategies introduced by the exoskeleton.

The entire simulation is executed within the MuJoCo (Multi-Joint dynamics with Contact) physics engine, which underlies the MyoSuite framework. This environment enables fast and physiologically plausible simulations of musculoskeletal dynamics, providing an efficient platform for inverse dynamics computations and torque tracking under both unassisted and exoskeleton-assisted conditions.

The estimation of the ATF is conducted using the `estimateATF.exe` tool, which integrates outputs from the inverse dynamics and muscle activation stages to produce a continuous tendon force profile over the gait cycle. This output is particularly important for quantifying the mechanical offloading provided by the AFO device, and serves as a key metric in evaluating the exoskeleton's efficacy in reducing tendon loading during locomotion.

4.4.5 Post-Processing and Export for Analysis

Finally, simulation outputs are post-processed for standardized comparison. All joint angle, muscle activation, and force trajectories are interpolated to a normalized 101-point gait cycle. These results are organized into structured matrices suitable for both statistical analysis and visual representation.

This standardization facilitates comparisons across conditions and platforms, including benchmark models such as OpenSim and Visual3D, allowing for robust cross-validation of the estimated joint kinematics and musculoskeletal dynamics under different walking scenarios.

Batch Automation with MyoSuite Tools

To ensure consistency and efficiency across trials, the simulation pipeline was automated using a suite of MyoSuite command-line executables:

- `embeddedIK.exe` – performs inverse kinematics from marker trajectories.
- `estimateATF.exe` – calculates Achilles tendon force from dynamic simulations.
- `getMarkerErrors.exe` – extracts marker tracking error metrics during IK fitting.
- `moveMarkerSet.exe` – transforms and aligns subject-specific marker sets.

These tools allowed for parallel processing of simulations across all subjects and trials, ensuring reproducibility and scalability in large-scale gait analysis.

4.5 OpenSim Processing Pipeline

OpenSim is an open-source and extensible software platform for simulating human movement using musculoskeletal (MSK) models. It offers a comprehensive library of biomechanical components, such as joints, muscles, and ligaments, and tools for customizing generic models based on subject-specific anatomical data. Using experimental inputs like marker trajectories, ground reaction forces (GRFs), and surface electromyography (sEMG), OpenSim enables detailed biomechanical analysis through inverse kinematics and forward dynamics. Ten gait cycles were analyzed for each condition and each speed, so the first step involved the manual cutting of the trials, in order to extract the single gait cycle to give as an input to the Opensim pipeline.

The overall processing pipeline, illustrated in Figure 4.7, outlines the steps from pre-processed experimental data to the estimation of Achilles tendon force (ATF). All analyses were performed using a custom MATLAB toolbox, *Batch OpenSim Processing Scripts (BOPS)*. This user-friendly tool, equipped with a graphical interface, automates batch processing of complex datasets using core OpenSim procedures: Inverse Kinematics (IK), Inverse Dynamics (ID), Residual Reduction Algorithm (RRA), and Computed Muscle Control (CMC).

The pipeline begins with subject-specific scaling of the MSK model, aligning it to individual anatomical dimensions. IK is then used to reconstruct movement from marker trajectories, providing estimates of joint kinematics. Based on these kinematics and external loads, the Inverse Dynamics (ID) step computes the net joint forces and moments required to produce the observed motion. RRA follows, integrating marker and GRF data to reduce dynamic inconsistencies by minimizing residual forces and refining model parameters.

Finally, CMC estimates the muscle activations needed to replicate the observed motion. In this study, we employed both standard CMC and an EMG-informed CMC approach, which incorporates experimental EMG data to better constrain the optimization.

This pipeline enables in-depth exploration of human biomechanics and muscle–tendon unit (MTU) dynamics. The following sections provide detailed descriptions of each processing step.

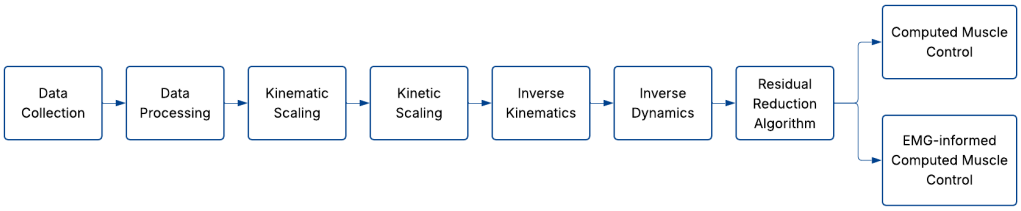

Figure 4.7: OpenSim pipeline for muscle force and tendon load estimation. Workflow used to estimate muscle activations and Achilles tendon force using OpenSim. The pipeline includes data collection, kinematic and kinetic scaling, inverse kinematics and dynamics, followed by the Residual Reduction Algorithm. Muscle force estimation is performed using either standard Computed Muscle Control (CMC) or an EMG-informed CMC approach.

4.5.1 Rajagopal Full-Body Musculoskeletal Model

The Rajagopal Full-Body Musculoskeletal Model is a comprehensive simulation framework designed to investigate muscle-driven human gait, including both walking and running [18]. It features 37 degrees of freedom (DOF) to define joint kinematics and incorporates 80 Hill-type muscle-tendon units in the lower limbs. These units act as massless actuators responsible for generating force and driving movement. Additionally, 17 ideal torque actuators are included to control upper body motion.

The model's muscle-tendon parameters are based on anatomical measurements from 21 cadaveric specimens and magnetic resonance imaging (MRI) data from 24 healthy young adults [18]. Muscle force generation is modeled using the Hill-type formulation, which includes two primary components: a passive elastic element representing viscoelastic properties of the tendon and passive tissues, and an active contractile element that produces force during muscle activation.

4.5.2 Scaling of the Musculoskeletal Model

To ensure subject-specific accuracy, the generic Rajagopal musculoskeletal model was scaled to match each participant's anthropometry. This scaling process involves both geometric and kinetic adjustments, aimed at adapting the model's dimensions and force-generating capabilities to individual anatomical and physiological characteristics.

Geometric Scaling

Geometric scaling is performed using a combination of measurement-based and manual scaling methods. The process begins by placing a set of experimental markers on anatomical landmarks of the subject using motion capture. Corresponding virtual markers are embedded in the unscaled model at equivalent anatomical locations. By comparing the average distances between experimental markers (from the `.trc` file) and virtual markers (in the model's default pose), scale factors for each segment are computed. For example, distances between pairs such as {`R.ASIS`, `R.Knee.Lat`} and {`L.ASIS`, `L.Knee.Lat`} are used to derive scale factors along the X, Y, and Z axes.

Kinetic Scaling

In addition to geometric scaling, a *kinetic scaling* step was performed to refine the force-generating capacity of the model's musculature. This was done by adjusting the *maximum isometric muscle force*, which is directly proportional to the specific tension value (in N/cm^2) used in the Hill-type muscle model.

The default Rajagopal model uses a muscle specific tension of 60 N/cm^2 [35], which enables the model to simulate high-performance tasks such as running. However, this can lead to an overestimation of muscle forces and joint power during lower-intensity activities like level walking. To address this discrepancy, we adopted a literature-recommended value of 30 N/cm^2 for walking studies, which better reflects physiological norms during submaximal effort.

This adjustment ensures that the simulated muscle forces and resulting joint kinetics are more consistent with empirical observations for typical walking trials, thereby enhancing the physiological accuracy of the simulation results.

4.5.3 Inverse Kinematics

The Inverse Kinematics (IK) tool estimates generalized coordinates at each time frame to align the model's virtual markers with the corresponding experimental markers collected during motion capture. This is achieved by solving a weighted least squares optimization problem that minimizes the distance between each pair of virtual and experimental markers throughout the recorded motion [20]. The importance of each marker in the optimization was adjusted by assigning custom weights, allowing us to emphasize anatomical markers over others, that are subducted to soft tissue artifacts or not perfectly placed [20].

The IK tool requires the following input files:

- **Subject-specific OpenSim model (.osim)**: A scaled version of a generic model (e.g., the Rajagopal model), adjusted using the Scale Tool to reflect the subject's anthropometry and including a set of virtual markers.
- **Experimental motion data (.trc)**: Marker trajectories recorded during a movement trial using a motion capture system.
- **Setup file (.xml)**: A configuration file specifying the paths to the model and motion data, along with solver parameters such as marker weights, which influence how closely the virtual markers follow the experimental ones. These weights are typically adjusted to prioritize markers on segments of interest.

The IK analysis produces a motion file (.mot) as output. This file contains time-varying joint kinematics and serves as input for subsequent steps in the analysis pipeline. The accuracy of this output depends on the marker tracking weights chosen during setup, which guide how well the model follows the recorded motion.

4.5.4 Inverse Dynamics

The Inverse Dynamics (ID) Tool in OpenSim computes the net joint moments and forces that produce a recorded motion, based on known kinematics and external loads. It applies Newtonian mechanics (i.e., $\mathbf{F} = m\mathbf{a}$) in reverse, using the model's motion and ground reaction forces (GRFs) to estimate the internal joint torques required to reproduce the observed movement.

This process requires three key inputs:

- **Motion file (.mot)**: Contains joint kinematics over time, typically obtained from the Inverse Kinematics (IK) analysis.
- **External loads file (.xml)**: Specifies the GRFs and their points of application, referencing a corresponding .mot file with the actual force data.
- **Subject-specific model (.osim)**: A scaled musculoskeletal model with accurate segment inertial properties. The model may include additional elements (e.g., muscles, ligaments), which can be excluded if not relevant to the analysis.

The output is a `.sto` file that stores the time histories of the generalized forces, joint torques and reaction forces, calculated by the tool. These results can be used in subsequent simulations or for evaluating joint loading during specific tasks. Accurate results depend on precise inputs, especially complete and correctly applied external forces.

4.5.5 Residual Reduction Algorithm

The Residual Reduction Algorithm (RRA) is an OpenSim tool designed to improve the dynamic consistency between experimental motion data and external forces, such as ground reaction forces (GRFs). Its primary goal is to reduce non-physical residual forces and moments, artifacts that arise due to modeling simplifications, mass distribution inaccuracies, and errors in marker-based motion capture data.

RRA achieves this by adjusting the model's torso mass properties and allowing small deviations in joint kinematics from the original inverse kinematics (IK) solution. These modifications aim to ensure that the simulated motion adheres more closely to Newtonian mechanics, thereby minimizing the need for artificial forces (residuals) at the model's base.

Inputs:

- **Motion file (.mot)**: Joint angles and translations over time, typically from IK.
- **External loads file (.xml)**: Specifies how GRFs are applied to the model.
- **Subject-specific model (.osim)**: Scaled musculoskeletal model with inertial properties.

- **Actuator file (.xml)**: Defines ideal torque and residual actuators for each degree of freedom.
- **Task file (.xml)**: Sets tracking priorities and weights for each coordinate.

Outputs:

- **Adjusted model (.osim)**: Model with a modified mass distribution.
- **State trajectories (.sto)**: Time-resolved joint angles and velocities after RRA.
- **Actuator controls (.xml)**: Control signals for the applied ideal actuators.
- **Residual summary (.sto/.txt)**: Average and peak residual forces and moments.
- **Position errors (.sto)**: Quantifies tracking deviation per coordinate.

RRA is a critical preprocessing step before running Computed Muscle Control (CMC), ensuring that the movement can be reproduced primarily by internal forces (e.g., muscles) rather than artificial residuals, leading to more physiologically meaningful simulation outcomes.

4.5.6 Computed Muscle Control (CMC)

Computed Muscle Control (CMC) is the final stage in the musculoskeletal simulation pipeline used to compute a set of muscle excitations and, more generally, actuator controls, that reproduce a desired movement while respecting biomechanical and physiological constraints. Given a set of joint kinematics and external forces (e.g., ground reaction forces), CMC drives a dynamic model to follow the target motion by solving a forward dynamics problem with control optimization at each time step.

The algorithm operates by combining proportional-derivative (PD) feedback control with static optimization. PD control calculates the accelerations needed to minimize the difference between simulated and experimental kinematics, while static optimization distributes the required joint torques across the available actuators (muscles, reserves, residuals) by minimizing a cost function based on actuator effort and tracking error. A short initialization phase (typically the first 0.030 s of simulation) is used to stabilize muscle states, and therefore the analysis is started slightly earlier than the time window of interest.

Inputs:

- **Subject-specific model (.osim)**: Includes adjusted torso mass center from RRA.
- **Adjusted motion file (.mot)**: Joint angles and translations from RRA.
- **External loads file (.xml)**: Specifies ground reaction forces and points of application.

- **Actuators file (.xml)**: Defines muscle, reserve, and residual actuators.
- **Control constraints file (.xml)**: Specifies activation limits and activation timing for actuators. This file was also used to model assistance provided by the ExoBoot device, by switching "on" the corresponding actuator only during periods of active torque delivery.
- **Task set file (.xml)**: Sets tracking weights for individual coordinates.
- **Setup file (.xml)**: Contains paths and global simulation settings.

Outputs:

- `controls.xml`: Time-resolved excitations for all actuators.
- `forces.sto`: Muscle forces and torques applied by reserve/residual actuators.
- `states.sto`: Simulated joint kinematics and muscle fiber states (activation, length).

CMC is particularly valuable when comparing simulated muscle activity with experimental electromyography (EMG). In this study, we employed EMG-informed actuator constraints to assist the simulation in the reconstruction of the muscle activations, as well as to simulate the torque provided by an external ankle-foot orthosis (ExoBoot). By incorporating this device into the model as a torque actuator and activating it according to experimental timing profiles, we ensured that assistance was realistically synchronized with the biological motion.

This approach allows for the generation of physiologically plausible simulations of assisted walking, enabling the evaluation of muscle force production, joint loading, and neuromuscular adaptations in response to wearable robotic interventions.

Chapter 5

Technical analysis: Comparison across softwares

5.1 Results

The objective of this section is to compare the outcomes of different simulation frameworks in order to understand their relative performance and determine which provides more accurate or physiologically meaningful results in the context of estimating the AT load. Specifically, we analyze outputs from **MyoSuite**, **OpenSim**, and **Visual3D** to assess the accuracy of joint kinematic reconstruction, the validity of estimated muscle activations, and the modulation of Achilles tendon loading and ankle torque generation across varying levels of assistance.

We begin by assessing inverse kinematics accuracy across the three platforms by comparing hip, knee, and ankle joint angles in the sagittal plane. Standard comparison metrics are employed, including range of motion (ROM), root mean square error (RMSE), normalized RMSE (NRMSE), and coefficient of multiple correlation (CMC). Visual3D, based on unconstrained marker reconstruction, is used as a reference due to its independence from model-based assumptions. MyoSuite and OpenSim are compared against this reference and against each other to quantify agreement and identify modeling differences.

The second part of this analysis focuses on lower-limb muscle activations. We compare experimental electromyography (EMG) data with simulated muscle activation outputs from both OpenSim and MyoSuite. Within OpenSim, we examine two approaches: traditional computed muscle control (CMC) and an EMG-informed CMC pipeline. Additionally, MyoSuite is evaluated as an independent solution. The goal is to identify the modeling framework that best reconstructs muscle activation patterns in terms of **shape, timing, and amplitude** of the signal, enabling the selection of the most physiologically relevant pipeline for downstream tendon force analysis.

Next, we analyze Achilles tendon force outputs generated from both OpenSim-based pipelines (CMC and CMC-EMG) to assess how simulated tendon loading varies with the level of external assistance provided by the AFO. This evaluation

supports the clinical objective of reducing AT loading and muscle demand during assisted walking.

This results section is organized to address the following aims:

- Assess inter-platform consistency in joint angle estimation.
- Evaluate the quality of muscle activation estimations across MyoSuite and OpenSim pipelines.
- Evaluate how different approaches behave in estimating Achilles tendon loading enabled by AFO assistance.

Both subject-specific and population-level analyses are presented to capture individual variability and overall trends in the dataset.

5.2 Inverse Kinematics Comparison Across Platforms

To assess the consistency and accuracy of inverse kinematics reconstruction in the sagittal plane, we compared joint angle estimations from **MyoSuite** and **OpenSim**, using **Visual3D** as a reference. Analyses were conducted for the hip, knee, and ankle joints during treadmill walking across two representative conditions: a normative walking condition without the AFO (No) and a fully assisted condition (150). Representative results are presented in Figure 5.1 for one subject and at the population level in Figure 5.2.

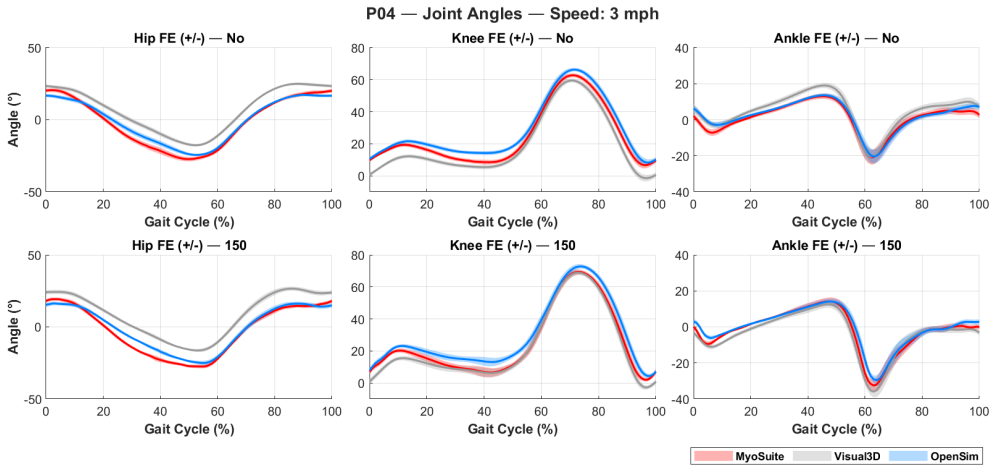

Figure 5.1: Sagittal plane joint angle estimation for subject P04 during treadmill walking. Hip, knee, and ankle flexion/extension (FE) angles are expressed in degrees over the gait cycle. MyoSuite estimations are shown in red, OpenSim in blue, and Visual3D in gray. Shade rapresent ± standard deviation Visual3D serves as the reference kinematic solution based on unconstrained marker reconstruction. Two levels of assistance are shown, No on top, 150 below.

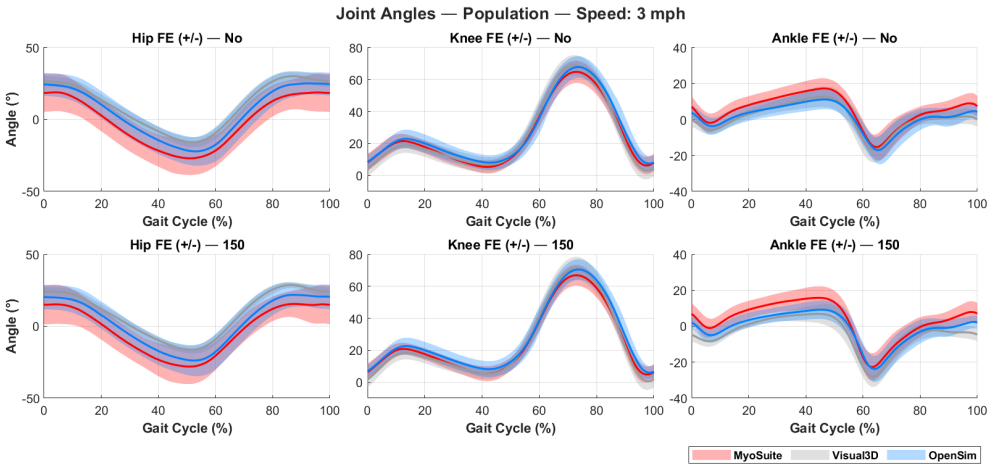

Figure 5.2: Population level sagittal plane joint angle estimation. Hip, knee, and ankle flexion/extension (FE) angles are expressed in degrees over the gait cycle. MyoSuite estimations are shown in red, OpenSim in blue, and Visual3D in gray.

Range of Motion (ROM) Analysis

Table 5.1 summarizes the average range of motion (ROM) across subjects for each platform during slow walking. These values were computed across the full gait cycle, averaging 10 left gait cycles per trial.

Hip OpenSim produced the highest average ROM ($48.70 \pm 5.06°$), followed by MyoSuite ($47.75 \pm 3.34°$), with Visual3D yielding the lowest values ($44.72 \pm 3.24°$). The elevated ROM in OpenSim may result from pelvis-thigh coupling and global optimization, while the reduced ROM in Visual3D likely reflects the use of anthropometric estimation for the hip joint center.

Knee ROM estimates were highly consistent across platforms.
MyoSuite ($63.56 \pm 9.47°$) and OpenSim ($64.73 \pm 6.59°$) aligned closely, while Visual3D estimated slightly higher values ($68.91 \pm 5.88°$), possibly due to unconstrained segmental tracking and swing-phase exaggeration. These results suggest strong robustness in knee kinematics across all models.

Ankle MyoSuite predicted the highest ROM ($36.25 \pm 6.01°$), followed by Visual3D ($34.72 \pm 4.13°$), with OpenSim predicting the lowest values ($31.43 \pm 4.56°$). These differences reflect model-specific handling of foot-ground contact, with OpenSim applying stricter constraints, and MyoSuite modeling more compliant foot dynamics. Visual3D, being unconstrained, often reflects heel and toe marker paths more directly.

5.2.1 Joint Angle Estimation During Stance Phase: MyoSuite vs OpenSim

To assess the agreement between MyoSuite and OpenSim in estimating sagittal plane joint kinematics, we computed standard waveform similarity metrics, root mean

Table 5.1: Range of motion (ROM) in degrees for each subject and joint. Values are expressed as mean ± SD.

Subject	Joint	MyoSuite	OpenSim	Visual3D
P00	Hip	47.88 ± 2.28	43.71 ± 3.07	43.91 ± 2.73
	Knee	62.80 ± 2.89	62.52 ± 2.20	65.17 ± 3.19
	Ankle	24.60 ± 3.13	23.18 ± 2.60	34.40 ± 2.85
P01	Hip	52.33 ± 2.77	52.40 ± 2.48	46.88 ± 1.99
	Knee	61.23 ± 2.65	59.56 ± 1.90	59.36 ± 2.53
	Ankle	31.36 ± 4.07	26.45 ± 3.67	28.83 ± 3.56
P02	Hip	41.35 ± 2.68	42.65 ± 1.28	41.01 ± 1.19
	Knee	64.35 ± 4.97	61.34 ± 4.40	65.23 ± 4.41
	Ankle	30.33 ± 6.38	27.42 ± 5.53	29.53 ± 4.35
P03	Hip	50.43 ± 2.36	52.18 ± 2.38	47.52 ± 1.70
	Knee	67.79 ± 2.52	66.86 ± 3.56	67.79 ± 2.92
	Ankle	36.09 ± 4.57	32.95 ± 4.14	38.77 ± 4.74
P04	Hip	46.54 ± 2.35	41.38 ± 1.68	42.81 ± 1.46
	Knee	62.59 ± 5.41	62.92 ± 5.72	66.28 ± 5.77
	Ankle	38.97 ± 6.96	37.54 ± 5.41	42.53 ± 5.73
P05	Hip	48.78 ± 1.09	47.97 ± 1.68	47.46 ± 1.74
	Knee	72.88 ± 1.76	75.26 ± 1.87	79.99 ± 2.22
	Ankle	36.37 ± 3.06	33.05 ± 2.76	34.72 ± 2.47
P06	Hip	48.18 ± 2.19	45.27 ± 1.63	46.65 ± 1.43
	Knee	72.07 ± 3.50	64.68 ± 3.33	71.93 ± 3.55
	Ankle	39.03 ± 6.11	36.00 ± 5.16	34.92 ± 6.18
P07	Hip	44.42 ± 2.26	48.63 ± 1.77	48.41 ± 1.56
	Knee	68.35 ± 2.27	65.53 ± 1.92	68.15 ± 2.03
	Ankle	38.43 ± 6.79	34.85 ± 6.18	34.46 ± 6.77
P08	Hip	50.47 ± 2.55	56.93 ± 2.82	46.86 ± 1.62
	Knee	74.03 ± 3.37	77.74 ± 4.19	77.96 ± 4.39
	Ankle	35.19 ± 4.44	27.60 ± 4.13	30.93 ± 4.57
S05	Hip	50.72 ± 2.47	54.46 ± 2.83	38.74 ± 1.87
	Knee	46.59 ± 2.80	59.67 ± 4.49	66.93 ± 3.54
	Ankle	41.00 ± 4.10	32.25 ± 3.75	34.12 ± 4.77
S06	Hip	44.20 ± 2.89	50.13 ± 3.64	41.67 ± 1.79
	Knee	46.50 ± 2.50	55.93 ± 3.30	69.27 ± 2.75
	Ankle	47.34 ± 7.97	34.43 ± 6.00	38.74 ± 8.06

Table 5.2: Range of Motion (ROM) estimates across platforms for hip, knee, and ankle (mean ± SD in degrees)

Joint	MyoSuite	OpenSim	Visual3D
Hip	47.75 ± 3.34	48.70 ± 5.06	44.72 ± 3.24
Knee	63.56 ± 9.47	64.73 ± 6.59	68.91 ± 5.88
Ankle	36.25 ± 6.01	31.43 ± 4.56	34.72 ± 4.13

square error (RMSE), normalized RMSE (NRMSE), coefficient of multiple correlation (CMC), and ROM error, for each joint during the stance phase. Results were computed per subject and aggregated across the population, pooling all assistance conditions to focus solely on modeling differences.

Subject-Level Analysis

Table 5.3 reports the stance-phase metrics for all subjects. The hip joint showed the largest variability in RMSE and CMC across subjects, highlighting its sensitivity to modeling assumptions such as joint center estimation and pelvis scaling. While some subjects (e.g., P04, P01) demonstrated high hip CMCs above 0.9, others like P02 and P07 fell well below, indicating inconsistent agreement across individuals.

The knee exhibited the most consistent agreement, with low RMSEs (generally $<5°$) and high CMCs (>0.85 for nearly all subjects), reflecting its relatively constrained motion and the robustness of its marker definition.

Ankle joint differences were intermediate, with slightly elevated RMSEs and NRMSEs compared to the knee. The CMC values were more variable, suggesting differences in shape, especially near toe-off, where modeling assumptions like compliant foot-ground contact in MyoSuite may contribute to more pronounced plantarflexion.

Population-Level Summary

The population-wide averages for each joint are reported in Table 5.4. These values support the subject-level findings: highest agreement at the knee, moderate differences at the ankle, and the largest discrepancies at the hip.

5.3 Muscle Activation Analysis

In this section, we evaluate how well MyoSuite, OpenSim CMC, and OpenSim CMC-EMG informed pipelines replicate the experimental EMG envelopes during treadmill walking at 3 mph in the **NoDephy** condition, i.e., without any exoskeletal assistance. By isolating this baseline condition, we aim to assess each model's intrinsic ability to reconstruct physiological activation patterns without the confounding effects of device support. The other conditions have been analyzed, but apart from a different level of activation given by the presence of the assistance, show consistent behaviours with what we have for the No condition, in terms of comparison across systems.

We analyze four muscles crucial to ankle function and Achilles tendon loading: Gastrocnemius Lateralis, Gastrocnemius Medialis, Soleus, and Tibialis Anterior. For each muscle, we assess whether the estimated activation waveforms correctly replicate the:

- **Shape** of the activation curve,
- **Amplitude** and modulation across the gait cycle,
- **Timing** of peak activation,

Table 5.3: Subject-level comparison metrics between MyoSuite and OpenSim during the stance phase. Values are reported as mean ± standard deviation.

Subject	Joint	RMSE (°)	NRMSE	CMC	ROM Error (°)
P00	Ankle	2.44 ± 0.3	0.13 ± 0.02	0.91 ± 0.04	4.01 ± 1.03
	Hip	7.9 ± 1.49	0.17 ± 0.03	0.94 ± 0.02	7.06 ± 0.65
	Knee	3.89 ± 0.65	0.15 ± 0.02	0.9 ± 0.03	3.37 ± 2.1
P01	Ankle	4.64 ± 0.7	0.18 ± 0.03	0.85 ± 0.04	6.43 ± 1.01
	Hip	26.11 ± 1.15	0.51 ± 0.04	0.59 ± 0.06	1.87 ± 1.08
	Knee	3.29 ± 0.33	0.1 ± 0.01	0.96 ± 0.01	4.79 ± 1.12
P02	Ankle	3.64 ± 0.28	0.14 ± 0.04	0.92 ± 0.02	5.46 ± 1.39
	Hip	7.43 ± 0.46	0.18 ± 0.02	0.95 ± 0.01	1.98 ± 1.59
	Knee	3.8 ± 0.4	0.11 ± 0.01	0.92 ± 0.01	4.17 ± 0.64
P03	Ankle	4.5 ± 0.93	0.15 ± 0.05	0.91 ± 0.04	4.1 ± 1.26
	Hip	16.19 ± 2.08	0.35 ± 0.05	0.82 ± 0.04	1.65 ± 1.31
	Knee	3.27 ± 0.31	0.08 ± 0.01	0.96 ± 0.01	4.73 ± 1.45
P04	Ankle	2.17 ± 0.3	0.07 ± 0.01	0.98 ± 0.01	4.36 ± 2.64
	Hip	4.46 ± 0.49	0.1 ± 0.02	0.98 ± 0.01	6.2 ± 0.91
	Knee	4.51 ± 0.34	0.15 ± 0.01	0.88 ± 0.02	2.1 ± 0.39
P05	Ankle	9.39 ± 1.23	0.32 ± 0.03	0.62 ± 0.09	6.2 ± 0.96
	Hip	10.38 ± 1.15	0.22 ± 0.02	0.91 ± 0.02	4.84 ± 1.57
	Knee	4.71 ± 0.22	0.11 ± 0.01	0.94 ± 0.01	1.19 ± 0.6
P06	Ankle	4.93 ± 0.46	0.18 ± 0.06	0.83 ± 0.07	5.67 ± 2.28
	Hip	33.97 ± 0.79	0.84 ± 0.05	0.31 ± 0.07	1.16 ± 0.39
	Knee	9.55 ± 0.35	0.24 ± 0.02	0.69 ± 0.05	7.78 ± 0.35
P07	Ankle	5.55 ± 1.23	0.21 ± 0.03	0.81 ± 0.06	6.07 ± 2.7
	Hip	16.6 ± 1.84	0.4 ± 0.03	0.77 ± 0.03	4.25 ± 1.81
	Knee	5.52 ± 0.3	0.16 ± 0.01	0.86 ± 0.01	5.73 ± 0.36
P08	Ankle	3.53 ± 0.44	0.12 ± 0.01	0.94 ± 0.01	7.88 ± 1.81
	Hip	3.61 ± 0.87	0.08 ± 0.02	0.99 ± 0.0	3.69 ± 1.38
	Knee	1.54 ± 0.32	0.04 ± 0.01	0.99 ± 0.0	1.21 ± 0.79
S05	Ankle	7.9 ± 0.81	0.23 ± 0.05	0.7 ± 0.06	9.16 ± 1.68
	Hip	6.83 ± 0.53	0.14 ± 0.01	0.96 ± 0.01	4.24 ± 2.69
	Knee	4.31 ± 0.64	0.15 ± 0.03	0.89 ± 0.04	5.34 ± 1.44
S06	Ankle	15.82 ± 1.87	0.47 ± 0.11	0.38 ± 0.13	10.32 ± 4.48
	Hip	4.78 ± 1.53	0.11 ± 0.04	0.97 ± 0.02	6.05 ± 2.91
	Knee	9.57 ± 0.16	0.41 ± 0.02	0.81 ± 0.05	5.84 ± 3.64

Table 5.4: Population-level comparison metrics between MyoSuite and OpenSim during stance phase.

Joint	**RMSE (°)**	**NRMSE**	**CMC**	**ROM Error (°)**
Hip	12.57 ± 9.81	0.28 ± 0.23	0.83 ± 0.21	3.91 ± 2.04
Knee	4.91 ± 2.51	0.15 ± 0.10	0.89 ± 0.08	4.21 ± 2.07
Ankle	5.87 ± 3.95	0.20 ± 0.11	0.80 ± 0.18	6.33 ± 2.05

- **Overall muscle recruitment pattern**.

The results are shown for each subject and for the population average (Figures 5.3 and 5.4). Shaded areas represent standard deviation across gait cycles.

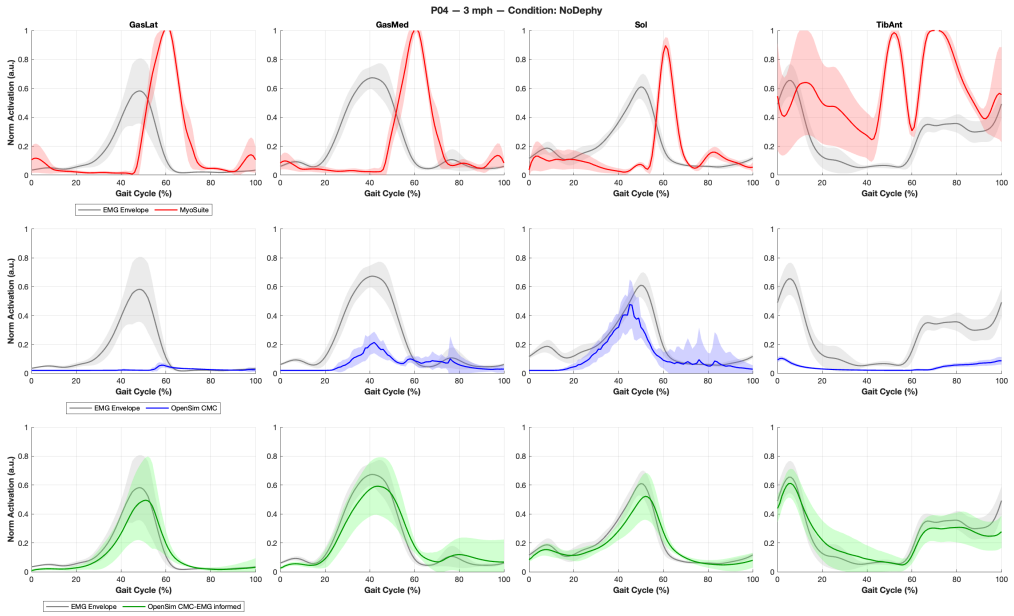

Figure 5.3: Muscle activation comparison for subject **P00** during treadmill walking at 3 mph in the **NoDephy** condition. The estimated muscle activations are shown for MyoSuite (red), OpenSim CMC (blue), and OpenSim CMC-EMG informed (green), and compared against the experimental EMG envelopes (gray). Each panel corresponds to one of the four analyzed muscles: Gastrocnemius Lateralis (GasLat), Gastrocnemius Medialis (GasMed), Soleus (Sol), and Tibialis Anterior (TibAnt).

5.3.1 Gastrocnemius Lateralis and Medialis

Both gastrocnemii contribute significantly to propulsion during late stance by generating plantarflexion torque and aiding knee flexion. Their EMG envelopes typically peak around 50–60% of the gait cycle.

CMC-EMG informed outputs consistently replicate this timing and magnitude, validating its use in simulating gastrocnemius-driven push-off.

In contrast, **OpenSim CMC** underestimates the activation of both heads of the gastrocnemius across subjects. This behavior likely stems from the optimizer prioritizing muscles with lower excitation cost or from overly simplified neuromuscular control assumptions in the absence of experimental priors.

MyoSuite usually captures the timing of peak activation but tends to overestimate amplitude and introduces non-physiological features such as double peaks (e.g., in subject P03). These artifacts may reflect the lack of a muscle-specific force normalization procedure and absence of kinetic scaling.

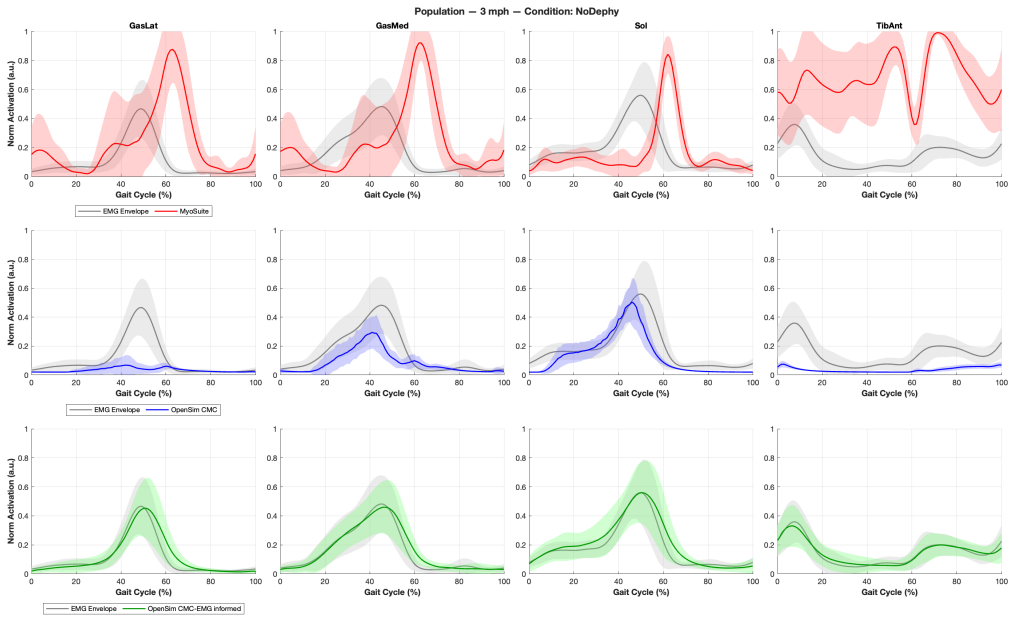

Figure 5.4: Population-level normalized muscle activations (mean ± SD) for the NoDephy condition at 3 mph. EMG envelopes are shown in gray; MyoSuite (red), OpenSim CMC (blue), and CMC-EMG informed (green).

5.3.2 Soleus

The soleus is the primary plantarflexor in mid to late stance and plays a central role in supporting body weight and enabling forward propulsion.

CMC-EMG informed simulations yield accurate reconstructions of soleus activity in terms of both timing (peak around 40–60%) and amplitude. **MyoSuite** shows more variability, but often captures peak value correctly, even though it does not perform well in estimating the peak time.

OpenSim CMC, however, slightly underestimates soleus activation amplitude. This again reflects the limitations of purely optimization-driven approaches without EMG constraints in accurately resolving the force contribution of key stabilizing muscles.

5.3.3 Tibialis Anterior

The tibialis anterior is active during early stance and swing, producing a characteristic double-peak EMG pattern (at 10–20% and 70–90% of the gait cycle) for dorsiflexion and foot clearance.

This double-burst behavior is well captured by the **CMC-EMG informed** pipeline.

MyoSuite exhibits exaggerated, prolonged activation of the tibialis anterior, sometimes spanning the entire gait cycle. This behavior is clearly non-physiological and suggests a breakdown in either torque tracking or neural control modeling. Notably, MyoSuite lacks subject-specific scaling and does not implement *kinetic scaling*, which likely contributes to overestimated joint torques and unnecessary

dorsiflexor engagement.

OpenSim CMC again fails to activate tibialis anterior sufficiently, producing flat or damped activation patterns in most subjects, which would compromise foot clearance and heel-strike control in dynamic simulations.

5.4 Achilles Tendon Load Estimation

The Achilles tendon plays a pivotal role during walking, primarily by transmitting forces from the triceps surae muscle group (gastrocnemius lateralis, gastrocnemius medialis, and soleus) to the calcaneus to generate plantarflexion torque during push-off. Accurate estimation of Achilles tendon force is thus contingent on reliable predictions of muscle force in these contributors, which in turn depend on the quality of muscle activation profiles derived from simulation.

5.4.1 Computation of Achilles Tendon Load

In this study, Achilles tendon force was computed as the sum of the muscle forces from the gastrocnemius lateralis, gastrocnemius medialis, and soleus. These forces were extracted from two different simulation pipelines:

1. **OpenSim CMC**, which predicts muscle forces based on a static optimization solution constrained by joint kinematics.
2. **OpenSim CMC-EMG informed**, which incorporates subject-specific EMG envelopes as soft constraints to guide the optimization toward physiologically plausible activation timing and magnitude.

The resulting tendon force waveforms, normalized by body weight, are shown in Figures 5.5 and 5.6 for each subject and for the group average, respectively.

5.4.2 Comparison Across Conditions

The Achilles tendon load curves exhibit the characteristic double-burst pattern associated with walking: a first peak during early stance and a second, higher peak during push-off (approximately 40–60 % of the gait cycle). These peaks are predominantly driven by the force output of the soleus and gastrocnemii.

Across all assistance conditions (NoDephy, DephyOff, Dephy50, Dephy100, Dephy150), the **CMC-EMG informed** pipeline consistently generates higher tendon forces than standard CMC, particularly during push-off. This reflects the higher activation magnitudes introduced by EMG-informed constraints, especially for the plantarflexors as previously observed in the activation analysis (Section 5.3).

One notable feature is the presence of a small **peak in tendon force** around mid-stance in many subjects under the CMC-EMG informed pipeline. This peak is absent in standard CMC simulations. Biomechanically, this may arise from a more physiological activation of the soleus early in stance, contributing to load support and forward propulsion before the main push-off phase. This early activation is typically

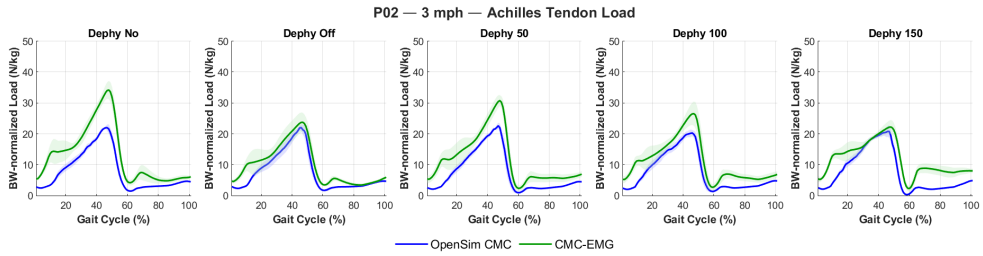

Figure 5.5: Achilles tendon load (normalized by body weight) across the gait cycle for subject P02 walking at 3 mph under five different AFO assistance conditions (NoDephy, DephyOff, Dephy50, Dephy100, Dephy150). Each subplot shows mean ± SD tendon load estimated using OpenSim Computed Muscle Control (CMC, blue) and EMG-informed CMC (green) across 10 left gait cycles. A reduction in peak tendon loading is observed with increasing assistance, particularly in the EMG-informed estimates.

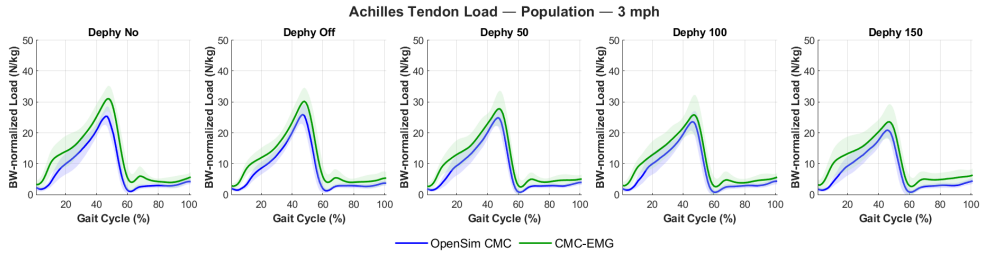

Figure 5.6: Population-level Achilles tendon load (normalized by body weight) across the gait cycle at 3 mph walking speed, shown for five AFO assistance conditions (NoDephy, DephyOff, Dephy50, Dephy100, Dephy150). Curves represent the mean ± SD across all subjects for OpenSim Computed Muscle Control (CMC, blue) and EMG-informed CMC (green) estimations. A consistent reduction in tendon load is observed during the push-off phase (40–60% gait cycle) with increasing assistance, particularly in EMG-informed simulations.

underrepresented in standard CMC due to cost function regularization and absence of EMG priors.

5.5 Discussion

This section discusses the interpretation of results from three core perspectives: (1) inverse kinematics estimation, (2) muscle activation profiles, and (3) Achilles tendon force modulation under AFO assistance. We reference the outcomes presented in Section 5.1 to contextualize the modeling choices, validation strategies, and biomechanical implications.

5.5.1 Kinematics: Platform Differences and Model Fidelity

Visual3D as Reference Framework

Visual3D was used as an unconstrained reference to estimate joint angles directly from marker trajectories, without enforcing joint constraints. The model adopts a full-body, six-degree-of-freedom (6-DoF) configuration, where joints maintain independent rotational and translational freedoms. No inverse kinematics optimization was applied, ensuring maximal fidelity to experimental marker data (Section 5.2).

In contrast, both OpenSim and MyoSuite constrain joint behavior through anatomical definitions and kinematic optimization routines. Notably, the hip joint centers in Visual3D are computed using the anthropometric method by Bell et al. [36], while OpenSim and MyoSuite use functional joint center estimation during inverse kinematics. Moreover, Visual3D models the pelvis as two separate hemipelves, whereas OpenSim and MyoSuite treat it as a rigid segment. These structural differences contribute to systematic offsets in estimated joint angles, particularly at the hip.

Modeling and Scaling Differences

OpenSim uses the Rajagopal musculoskeletal model, which is scaled to subject anthropometry using geometric marker-based methods and virtual marker registration. Marker weights are adjusted to reduce the impact of soft tissue artifacts. The scaled model is consistent across trials for each subject.

In contrast, MyoSuite performs internal scaling and kinematic estimation *per trial*, without user-defined marker weighting. This can result in inconsistencies in joint center placement across trials. The impact of this is evident in subjects S05 and S06, where marker placement on technical clusters (due to AFO interference) introduced additional scaling artifacts. These inconsistencies increased the deviation of MyoSuite and OpenSim from the Visual3D reference but preserved relative agreement between each other.

Kinematic Interpretation and Conclusions

Across joints, the knee displayed the highest consistency between MyoSuite and OpenSim, with excellent waveform alignment and comparable ROM estimations (Section 5.2). The ankle showed moderate variability, particularly during late stance, due to platform-specific foot modeling. The hip exhibited the largest discrepancies, likely due to upstream differences in pelvis modeling and scaling procedures.

These results justify the selection of Visual3D as the unconstrained reference and reinforce the validity of OpenSim and MyoSuite kinematics for downstream use, provided the differences in scaling and joint estimation are acknowledged. Across all joints, the computed kinematic errors remained within acceptable thresholds reported in the literature. For instance, root mean square errors (RMSE) below 6° and CMC values above 0.75 are commonly considered good to excellent for joint angle comparisons [37, 38, 39].

5.5.2 Muscle Activations: Physiological Validity and Model Assumptions

Kinetic Scaling and Force Capacity

A key distinction between platforms lies in the treatment of muscle strength. In OpenSim, following geometric scaling, a kinetic scaling step was implemented by adjusting muscle specific tension from 60 N/cm^2 to 30 N/cm^2 [35], reflecting force capabilities appropriate for walking. This ensured that muscle-generated joint torques remained within physiological ranges and avoided overestimation (Section 5.3).

MyoSuite, on the other hand, lacks kinetic scaling. The default muscle capacities remain unadjusted, potentially leading to overactivation or antagonistic co-contraction in the optimization results. This was particularly evident in the tibialis anterior and gastrocnemius, whose activation patterns deviated substantially from both physiological norms and experimental EMG envelopes.

Activation Source Selection for Tendon Estimation

Based on these findings, we excluded MyoSuite muscle activations from tendon force estimation. Although timing was sometimes accurate, activation amplitudes and shapes, especially in the tibialis anterior, were inconsistent with expected neuromuscular control.

We retained both OpenSim CMC and EMG-informed CMC activations for tendon force simulation. While standard CMC tended to underestimate activation amplitudes, it preserved physiological timing and provided a reliable control strategy baseline. EMG-informed CMC, incorporating experimental envelopes, showed the best alignment with physiological activation in both amplitude and timing.

Thus, for all downstream tendon force analyses, EMG-informed CMC was used as the primary activation source, with standard CMC used for reference. This decision

ensured accurate and interpretable force generation patterns while enabling a direct comparison between optimization-based and EMG-driven simulations.

This decision ensured accurate and interpretable force generation patterns while enabling a direct comparison between optimization-based and EMG-driven simulations. Previous studies have shown that RMS differences of 0.1–0.2 a.u. and timing differences within 10% of the gait cycle are typical when comparing simulated to experimental EMG, and are considered acceptable for lower-limb gait analyses [40].

Biomechanical Implications of Activation Patterns

Accurate muscle activation is essential for valid estimation of joint torques, contact forces, and tendon loads. Underestimations in plantarflexor activation or exaggerated antagonist activity may distort push-off dynamics. For instance, incorrect tibialis anterior timing affects swing clearance and heel strike control, while misestimations in the gastrocnemius or soleus impair propulsion.

By selecting physiologically valid activation patterns (OpenSim CMC and EMG-informed), we ensured that simulated muscle–tendon dynamics remained realistic and interpretable, especially when evaluating device-related modulations.

5.5.3 Tendon Load Modulation: Impact of AFO Support

Observed Reductions with EMG-Informed Inputs

Across subjects, Achilles tendon force estimated via EMG-informed CMC revealed consistent reductions with increasing AFO assistance, particularly during push-off (Section 5.4). Subjects such as P01, P02, and P06 exhibited clear decreases in peak tendon load from Dephy Off to Dephy150, demonstrating the mechanical offloading effect of the exoskeleton.

These reductions were most apparent in the EMG-informed condition, which directly reflects experimental neuromuscular dynamics. Reported errors in tendon force estimations, such as peak deviations within 10–20% of body weight and RMS errors under 3Nm, are in line with those found in prior EMG-informed musculoskeletal simulations of walking[41]. Our results fall within this validated range, supporting the reliability of the computed unloading effects.

Limitations of Standard CMC in Capturing Unloading

Standard CMC simulations, while temporally aligned, consistently underestimated activation amplitudes, leading to reduced force predictions even under baseline conditions. As a result, CMC failed to reflect the progressive unloading effect of the AFO. This finding highlights the necessity of EMG-informed activations to detect assistance-driven changes in tendon load, especially in submaximal tasks such as walking.

Activation–Force Coupling and Residual Force Phenomena

In Hill-type muscle models, activation levels directly influence muscle force generation. Consequently, underestimations in activation (as seen with CMC) translate to lower tendon forces. By contrast, EMG-informed simulations maintained activation profiles that matched both the magnitude and timing of expected neuromuscular control.

A notable feature in EMG-informed simulations was the presence of a secondary force peak during swing. This may reflect residual activation in the soleus or gastrocnemius, carried over from late stance, due to electromechanical delay and the slow deactivation of slow-twitch fibers. This phenomenon underscores the value of EMG-driven modeling in capturing fine-grained neuromuscular dynamics.

Summary and Rationale for Model Choice

In summary, EMG-informed simulations provided the most accurate estimation of tendon forces across assistance conditions, capturing both the expected unloading effect and the physiological characteristics of muscle recruitment. Standard CMC, while informative in timing, lacked the amplitude fidelity necessary to evaluate force modulation.

- EMG-informed simulations captured consistent reductions in Achilles tendon load during push-off with increasing AFO support.
- Secondary peaks in the force profiles likely reflect residual muscle activation beyond toe-off, captured only with EMG-driven inputs.
- Accurate force estimation depends on selecting activation sources that preserve both timing and magnitude fidelity.

These conclusions guided our selection of EMG-informed CMC as the primary framework for tendon force evaluation in this study.

Chapter 6

Impact of Ankle-Foot Orthosis Assistance on Neuromuscular and Biomechanical Parameters

This section investigates the clinical objective of the study: quantifying the biomechanical and neuromuscular effects of a powered ankle-foot orthosis (AFO) across varying levels of assistance during treadmill walking at two different levels of speed. The analysis focuses on how external support influences muscle activation, joint kinetics, and Achilles tendon loading, with particular attention to the push-off phase of gait, a critical period for propulsion and forward progression.

The evaluation is organized around three key biomechanical themes:

1. **Neuromuscular response:** We examine the modulation of muscle activation levels across AFO conditions, focusing on both *plantarflexors* (e.g., soleus, gastrocnemii) and *dorsiflexors* (e.g., tibialis anterior). A decrease in activation with increasing assistance would indicate effective mechanical offloading and potential neuromuscular adaptation.

2. **AFO torque integration:** The correct implementation of the exoskeleton torque profile within the OpenSim simulation framework is verified to ensure that the device's mechanical support is accurately represented. This validation step is essential to isolate AFO-induced changes in joint kinetics from simulation artifacts.

3. **Achilles tendon load:** We assess changes in the Achilles tendon force across conditions, as a surrogate for triceps surae loading. A consistent reduction in tendon force with increased AFO support would support the device's efficacy in offloading the plantarflexors and mitigating strain on the Achilles tendon.

The **NoDephy** (no AFO) condition is used as the physiological baseline, representing unassisted natural gait. All subsequent comparisons are referenced to this state to evaluate the effect of both passive and active exoskeletal support. The

DephyOff condition (AFO worn but unpowered) is particularly informative as it allows us to isolate the influence of passive device properties (e.g., inertia, stiffness, physical constraint) on gait mechanics, independent of active torque application.

In addition to examining propulsion-related dynamics, we specifically investigate the behavior of the **tibialis anterior**, the primary ankle dorsiflexor. Its function during early stance and swing phase is critical for foot clearance and controlled foot contact. Evaluating both activation patterns and generated forces in the dorsiflexors allows us to determine whether increasing plantarflexor support via the AFO induces compensatory reductions or deficits in dorsiflexor activity, an important consideration for overall gait symmetry and safety.

Lastly, the relationship between muscle activation and tendon force is explicitly addressed. Since tendon force is the resultant of the sum of individual muscle forces acting in series, any change in neural activation (especially under EMG-informed conditions) directly modulates tendon load. Understanding this interplay is essential for interpreting how neuromechanical control strategies adapt to external assistance and for designing effective rehabilitation or support protocols.

6.1 EMG Activation Reductions Across Assistance Levels During Push-Off

This section analyzes the impact of AFO torque on muscle activation during the gait cycle, with a specific focus on the **push-off phase** (40–60% of the gait cycle), where the orthosis is actively delivering mechanical assistance. We evaluated reductions in normalized EMG signals across the triceps surae muscles, gastrocnemius lateralis, gastrocnemius medialis, and soleus, as well as the tibialis anterior, to assess potential compensatory activation. Analysis was conducted at both walking speeds: 3 mph and 3.3 mph.

Population-Level Results

Figures 6.1 and 6.2 show the average EMG profiles and percentage reductions in root mean square (RMS) and area under the curve (AUC) during push-off.

Key findings include:

- **Soleus** showed the largest and most consistent reductions in EMG during push-off. At 3mph speed, RMS reductions increased from 9.2% at 50% assistance to 25.2% at 150%. At 3.3mph speed, reductions were slightly more pronounced, reaching 27.7% at 150%.
- **Gastrocnemius lateralis** exhibited moderate reductions. At 3.3 mph, the reduction increased from 3.4% at 50% to 9.5% at 150%. At 3 mph, reductions were 3.4%, 13.8%, and 17.9% at 50%, 100%, and 150%, respectively.
- **Gastrocnemius medialis** presented more variable behavior. Reductions remained below 10% at all levels in the 3.3 mph condition.

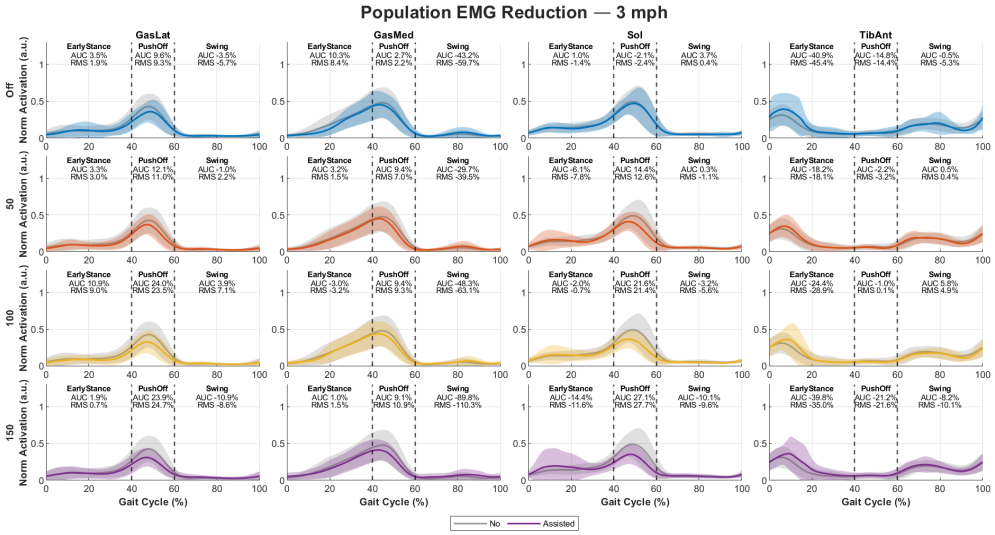

Figure 6.1: Normalized EMG activation profiles are shown for four muscles, lateral gastrocnemius (GasLat), medial gastrocnemius (GasMed), soleus (Sol), and tibialis anterior (TibAnt), cross four exosuit assistance levels: Off (top row), 50% (second row), 100% (third row), and 150% (bottom row). Shaded areas represent the standard error across subjects. Vertical dashed lines denote approximate gait cycle phase transitions: Early Stance, Push-Off, and Swing. For each phase, the Area Under the Curve (AUC) and Root Mean Square (RMS) percentage change are reported for the Assisted condition relative to the No Assistance condition. Negative values indicate a reduction in muscle activity.

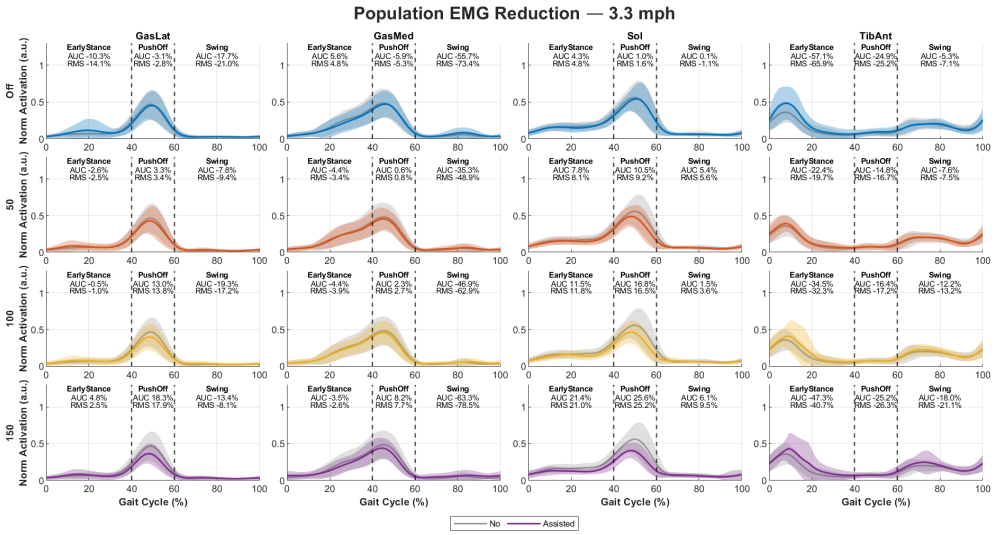

Figure 6.2: Population-level EMG activation profiles and reduction metrics for four muscles (Gastrocnemius Lateralis, Gastrocnemius Medialis, Soleus, Tibialis Anterior) during treadmill walking at 3.3 mph across increasing levels of AFO assistance (Dephy Off, 50, 100, 150). For each condition, the mean ± SD normalized activation (a.u.) is shown over the gait cycle, comparing the unassisted baseline (gray) to the assisted condition (colored).

- **Tibialis anterior** generally showed no increase in activation and was often reduced, with RMS decreasing by up to 14.4% at 150% in the 3.3 mph condition.

Subject-Specific Results

Figures 6.3 and 6.4 illustrate results from a representative subject. Reductions varied substantially across individuals:

- **P02, P04, and S05** showed consistent and large reductions across all plantarflexors at both speeds. Notably, S05 exhibited over 40% RMS reduction in GasLat at 150% assistance, alongside parallel reductions in ATF.
- **P01 and P07** displayed mixed responses. P01 showed minimal modulation in GasMed and TibAnt across speeds. P07 presented GasLat and Sol reductions at 3 mph, but irregular GasMed activation bursts post push-off at 3.3 mph, potentially due to altered MVC calibration or prolonged deactivation.
- **P08 and S06** were highly responsive at high assistance. S06 showed a 32% Sol RMS reduction and 13.8% TibAnt reduction at 150%. P08 displayed reductions exceeding 40% across GasLat, GasMed, and Sol, and up to 77% in TibAnt.
- **Secondary peaks** in GasLat or GasMed post push-off were observed in a few subjects (e.g., P04, P06), potentially due to compensatory activity or slow muscle deactivation. These were isolated and not widespread.

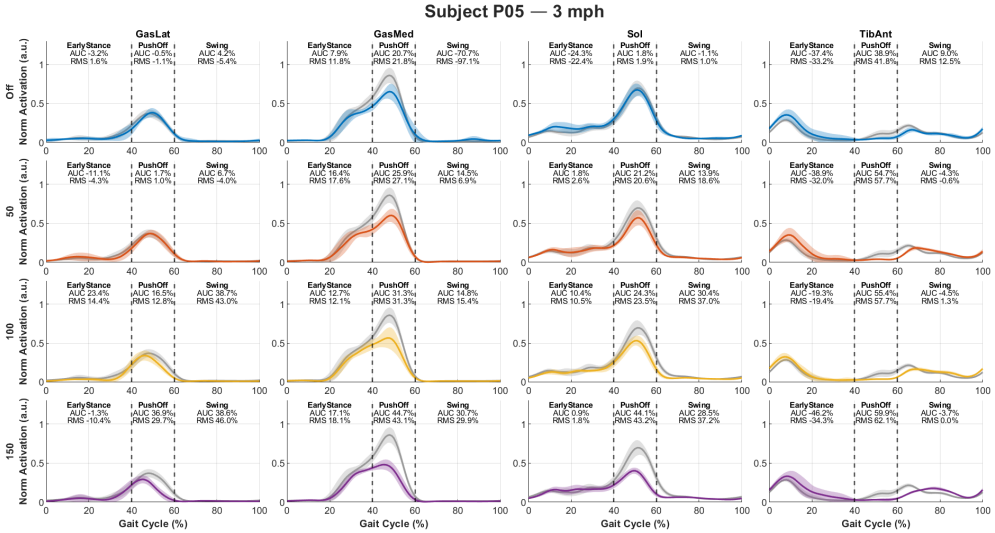

Figure 6.3: Subject P05, EMG activation profiles and phase-specific reduction metrics at 3 mph walking speed. Normalized EMG signals (mean ± SD across 10 left gait cycles) are shown for four muscles (Gastrocnemius Lateralis, Gastrocnemius Medialis, Soleus, Tibialis Anterior) across four AFO assistance conditions (Dephy Off, 50, 100, 150). The gray line represents the unassisted baseline (NoDephy). Vertical dashed lines mark the Early Stance, Push-Off, and Swing phases. Reductions in muscle activation are quantified using Area Under the Curve (AUC) and Root Mean Square.

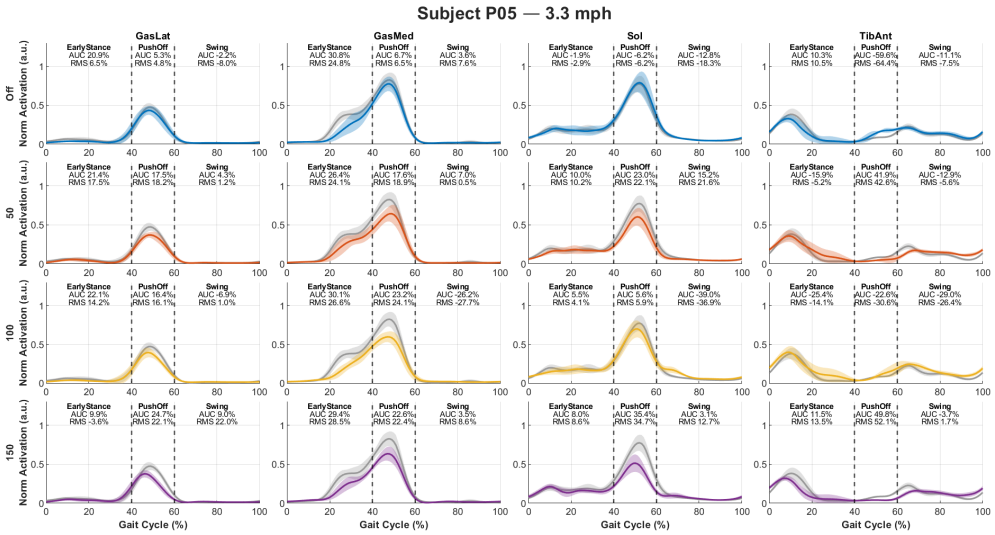

Figure 6.4: Subject P05, EMG activation profiles and phase-specific reduction metrics at 3.3 mph walking speed. Normalized EMG signals (mean ± SD across 10 left gait cycles) are shown for Gastrocnemius Lateralis, Gastrocnemius Medialis, Soleus, and Tibialis Anterior across increasing AFO assistance levels (Dephy Off, 50, 100, 150). The unassisted baseline (NoDephy) is shown in gray for reference. Dashed vertical lines delineate the gait phases.

6.2 Achilles Tendon Force Reduction Across Assistance Levels

This section presents the analysis of Achilles tendon force (ATF) during gait under different levels of AFO assistance, estimated through CMC-EMG simulations. The primary goal is to evaluate the mechanical offloading provided by the AFO during the **push-off phase** (40–60% of the gait cycle), where the device actively contributes to propulsion.

Figures 6.5 and 6.6 show the average population profiles at 3 mph and 3.3 mph, respectively.

Population-Level Reductions

At 3 mph:

- Off: 2.2% reduction (±3.4%)
- 50%: 9.3% (±6.3%)
- 100%: 16.3% (±7.0%)
- 150%: 22.6% (±9.7%)

At 3.3 mph:

- Off: 2.1% (±3.6%)
- 50%: 16.2% (±6.5%)

- 100%: 18.0% (±6.2%)
- 150%: 25.5% (±9.1%)

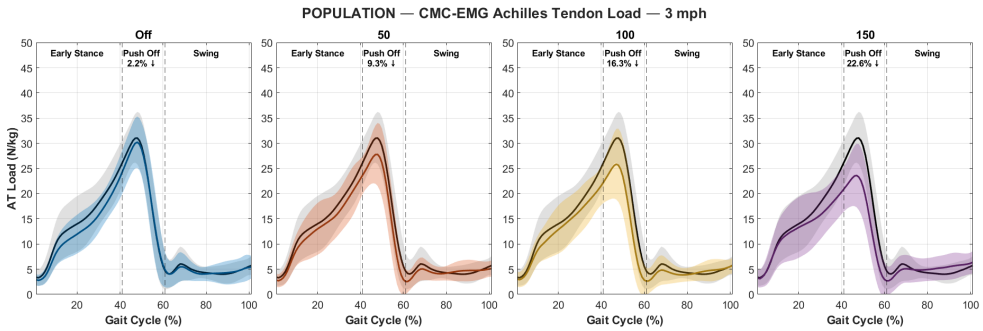

Figure 6.5: Population-average Achilles tendon load estimated via EMG-informed CMC at 3 mph for four AFO conditions. The black curves represent the mean NoDephy baseline, and the colored curves represent assisted conditions (Dephy Off, 50, 100, 150). Shaded regions denote inter-subject variability. Vertical lines segment the gait into Early Stance, Push-Off, and Swing phases. Annotated percentages indicate the average reduction in peak tendon load during push-off for each assisted condition compared to the baseline.

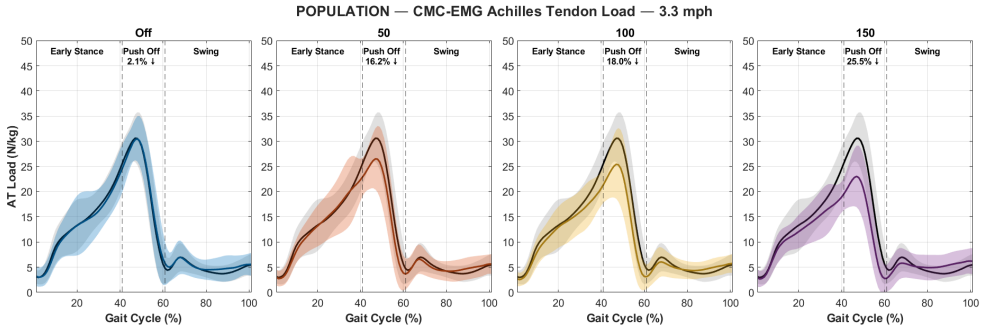

Figure 6.6: Achilles tendon load across the population at 3.3 mph, estimated using EMG-informed CMC for increasing levels of AFO support. Baseline (NoDephy) curves are shown in black, with assisted conditions overlaid in color. Shaded areas represent between-subject standard deviations. Vertical dashed lines mark gait phases, and annotated values indicate the percentage reduction in peak tendon load during push-off relative to baseline. A consistent unloading trend is observed with higher levels of assistance.

Subject-Specific Reductions

Figures 6.7 and 6.8 show data from a representative subject. Notably:

- **P02, P06, and P07** showed peak ATF reductions up to 35–40% at high assistance levels.
- **P00, P03, P08, and S05** exhibited moderate, consistent reductions (20–25% at 150%).

- **S06 and P04** showed minimal reductions (<10% at 150%), possibly due to poor EMG quality, fit, or gait pattern variability.
- **P01** displayed inconsistent reductions and secondary ATF peaks beyond push-off.

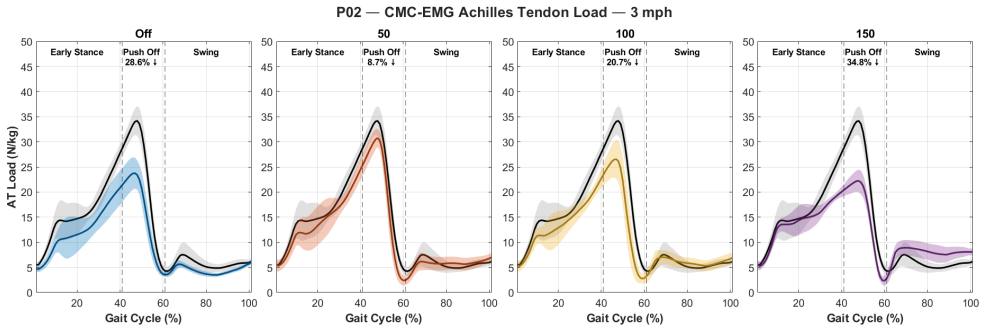

Figure 6.7: Achilles tendon load for subject P02 at 3 mph, estimated using EMG-informed CMC. Each subplot corresponds to one AFO condition (Dephy Off, 50, 100, 150) and overlays the assisted (colored) and baseline (black) tendon load profiles. Shaded areas denote variability across gait cycles. The peak reduction in tendon load during push-off is annotated above each plot, highlighting a progressive unloading effect with increasing AFO assistance.

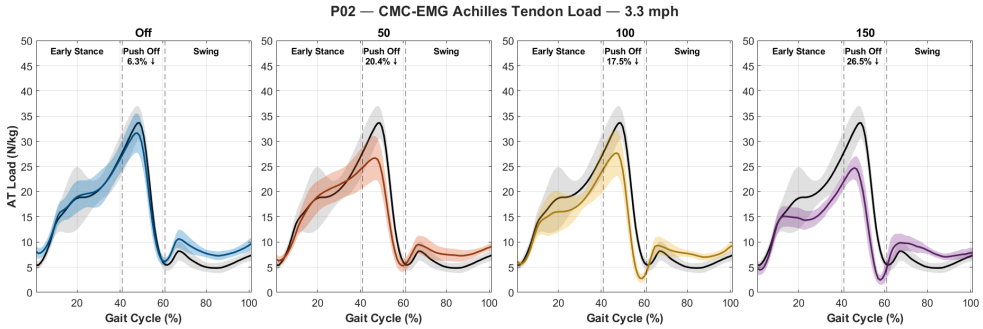

Figure 6.8: Achilles tendon load estimated with EMG-informed CMC for subject P02 walking at 3.3 mph under increasing AFO assistance (Dephy Off, 50, 100, 150). Each subplot shows the mean ± SD of normalized tendon force over the gait cycle. The black line represents the unassisted baseline (NoDephy), while the colored line shows the assisted condition. Vertical dashed lines indicate Early Stance, Push-Off, and Swing phases. Percentage values indicate peak Achilles tendon load reductions during push-off relative to baseline.

Population-Level Reductions During Push-Off

To further characterize the mechanical and neuromuscular offloading provided by the AFO, we quantified the percentage reduction in both EMG RMS signals and Achilles tendon force (ATF) during the **push-off phase** (42–61% of the gait cycle) across all subjects. Figures 6.9 and 6.10 report the mean ± standard deviation of the reduction values for each assistance level (50%, 100%, 150%) at both walking speeds

(3 mph and 3.3 mph), separately for the lateral gastrocnemius, medial gastrocnemius, and soleus muscles, along with the corresponding ATF reduction.

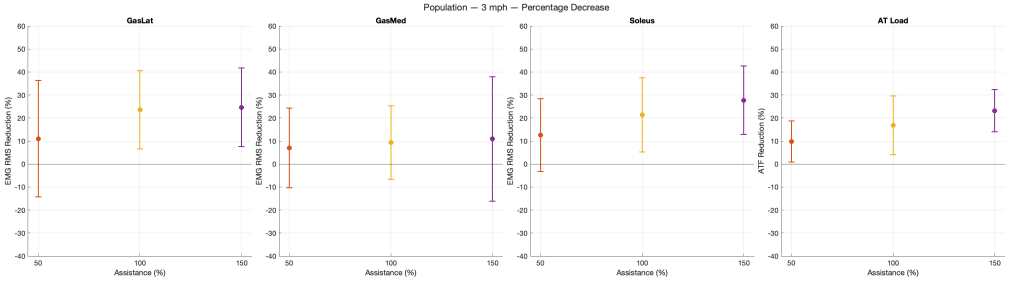

Figure 6.9: Population-level percentage reduction in EMG RMS activity and Achilles tendon force (ATF) during the push-off phase (42–61% of the gait cycle) for each AFO assistance level (50%, 100%, 150%) at **slow walking speed** (3 mph). Results are shown for three plantarflexor muscles, lateral gastrocnemius (GasLat), medial gastrocnemius (GasMed), and soleus, as well as for ATF. Error bars indicate standard deviation across subjects. The plots show a clear increase in tendon offloading and EMG reduction with increasing assistance, especially for the soleus.

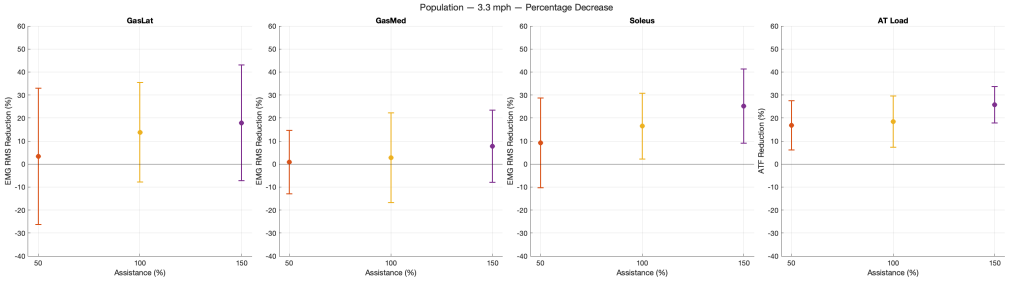

Figure 6.10: Population-level percentage reduction in EMG RMS activity and Achilles tendon force (ATF) during the push-off phase (42–61% of the gait cycle) for each AFO assistance level (50%, 100%, 150%) at **fast walking speed** (3.3 mph). Results are shown for three plantarflexor muscles, lateral gastrocnemius (GasLat), medial gastrocnemius (GasMed), and soleus, as well as for ATF. A consistent offloading pattern is observed with increasing AFO assistance, with the soleus again showing the highest EMG reduction across subjects.

At both speeds, an increasing trend in ATF reduction is observed with rising assistance levels, reaching approximately 25–30% reduction at 150%. This supports the efficacy of the AFO in mitigating the mechanical load borne by the Achilles tendon during push-off.

In terms of muscle activity, the soleus consistently shows the highest EMG reduction across both speeds, reaching values above 20% at 150% assistance. The gastrocnemii exhibit more variable patterns, with moderate reductions that tend to increase with assistance but are accompanied by larger inter-subject variability, particularly for the medial head. These results reflect differential muscle contributions during push-off and highlight how plantarflexor unloading is achieved both through direct mechanical support and a corresponding decrease in neuromuscular drive.

Taken together, these findings confirm that the AFO effectively reduces both

muscle effort and tendon loading in a dose-dependent manner, with the strongest effects observed at the highest assistance level. The agreement between EMG and ATF reductions provides compelling validation of the device's offloading capability during the most demanding phase of gait.

6.2.1 Validation of AFO Torque Implementation

To verify the correct integration of the ankle torque information provided by the exoskeleton into the musculoskeletal simulations, we compared the **input AFO torque profiles** (as derived from the recorded exoskeleton command signals) with the **output AFO torques** estimated from the simulations. Figure 6.11 displays this comparison across the three levels of active assistance (50%, 100%, and 150%) for a representative subject, averaged across ten left gait cycles.

Each subplot shows the mean ± standard deviation of the input (gray shaded area) and simulated output (pink shaded area) torque profiles over the gait cycle. Qualitatively, we observe that the output torques closely follow the shape and magnitude of the input profiles, especially during the stance phase, where the AFO is actively assisting.

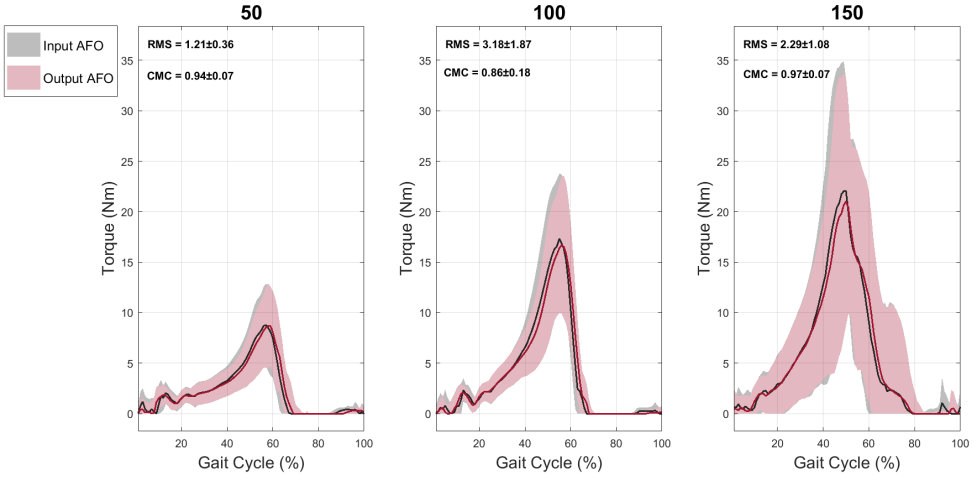

Figure 6.11: Comparison between input (gray) and output (red) ankle torque profiles across the gait cycle for three levels of AFO assistance: Dephy50, Dephy100, and Dephy150. Each subplot shows mean ± SD torque (Nm) over 10 gait cycles. Input torque represents the reference signal provided to the AFO controller, while output torque corresponds to the measured actuation response. The agreement between signals is quantified using Root Mean Square Error (RMS) and Coefficient of Multiple Correlation (CMC), reported in each subplot. Higher assistance levels yield greater peak torques, with consistently high CMC values indicating accurate reproduction of the target signal.

Agreement was high:

- RMSE remained under 3.2 Nm across all levels (e.g., 1.21 ±0.36 Nm at 50%, 3.18 ±1.87 Nm at 100%, and 2.29 ±1.08 Nm at 150%)

- CMC values exceeded 0.94 at 50% and 150% (0.94 ±0.07, 0.97 ±0.07), with slightly lower agreement at 100% (CMC = 0.86 ± 0.18)

6.3 Discussion

Neuromuscular Effects of AFO Assistance

The observed reduction in triceps surae muscle activity with increasing AFO support confirms that the exoskeleton effectively decreases the need for active plantarflexor recruitment during push-off. This effect was most pronounced in the soleus, a key contributor to propulsion. Interestingly, at the highest level of assistance, we also observed increased tibialis anterior activity during early stance, suggesting a degree of co-contraction with the soleus under these conditions. This pattern may reflect a neuromuscular strategy to stabilize the ankle joint in response to the elevated external torque provided by the AFO. Overall, these findings are consistent with previous reports of EMG reductions under powered assistance [42, 43], while also highlighting the potential for altered activation patterns at higher support levels.

Mechanical Offloading of the Achilles Tendon

EMG-informed simulations revealed that tendon load reductions scaled with AFO assistance, reaching up to 25.5% at high assistance levels. This result supports the AFO's capacity to offload the plantarflexor–tendon unit in a dose-dependent and phase-specific manner. Comparable reductions in simulated tendon force have been observed in studies combining exoskeletons with EMG-informed modeling [40, 41].

Inter-Subject Variability and Clinical Implications

Although group-level trends were clear, individual responses varied. Some participants showed minimal change in ATF or EMG with assistance, highlighting the influence of gait strategy, AFO fit, or neuromechanical adaptation. Additionally, differences in body weight and height likely contributed to how the same levels of external assistance affected each subject, altering the mechanical demands and resulting muscle and tendon responses. This variability underscores the importance of subject-specific modeling and justifies future studies on personalized AFO control strategies.

Validation of Torque Implementation

Simulation outputs closely matched recorded AFO torque profiles, with low RMSE and high CMC values across all levels. This confirms that the mechanical input from the device was faithfully integrated into the musculoskeletal simulation, isolating observed changes as genuine effects of assistance.

Conclusion

This study confirms that powered AFO assistance reduces both neuromuscular activation and Achilles tendon loading in a dose-dependent fashion. The findings support the hypothesis that mechanical support during push-off reduces plantarflexor effort and strain, without inducing detrimental compensation. These results provide a robust basis for the future design and control of assistive devices aimed at reducing lower-limb workload during gait.

Chapter 7

Limitations and Future Directions

Modeling Limitations and Experimental Constraints

While the present study provides promising evidence of the AFO's capacity to reduce Achilles tendon loading and muscle activation during walking, several modeling assumptions and experimental limitations should be considered when interpreting the results.

Simplified Modeling of the AFO

The ankle torque provided by the exoskeleton was modeled as an ideal actuator applying torque at a single joint coordinate. This simplification does not account for the complex biomechanical interaction between the human limb and the device, including factors such as misalignment, soft tissue deformation, or contact dynamics at the cuff–leg interface. As such, although the net torque application is replicated in the simulation, the internal joint and muscle forces might differ from those that would occur under real-world human–robot interaction. Future implementations should consider a more realistic interface modeling, for example using contact models or elastic couplings, to better approximate the effect of the exoskeleton on internal musculoskeletal loading.

Treadmill Locomotion Effects

Data collection was performed on an instrumented treadmill to enable synchronized motion capture and ground reaction force acquisition. While this setup is advantageous for clean, continuous data acquisition, it introduces an inherent limitation: walking on a treadmill lacks the forward propulsion typically present in overground walking. This could affect muscle activation strategies and potentially bias the simulation results, as the OpenSim algorithm assumes a forward walking intent. Caution is therefore advised when generalizing results from treadmill-based simulations to real-world overground walking conditions.

EMG Normalization Methodology

EMG signals were normalized using maximum voluntary contraction (MVC) tasks performed for each target muscle. However, the MVC procedure involved isolated contractions, which may not have elicited the true isometric maximal force for each muscle, especially in deep or synergistic muscles. This introduces a potential source of error in EMG normalization. While we partially mitigated this limitation by kinetically scaling the musculoskeletal model, thereby allowing muscles to express their subject-specific maximum isometric force, this approach does not correct for non-optimal MVC recordings. Future studies could explore dynamic normalization techniques or use standardized isometric protocols for more reliable EMG scaling.

Limited Muscle Recordings

EMG data were collected from only four muscles per leg (lateral gastrocnemius, medial gastrocnemius, soleus, and tibialis anterior). While this limited dataset may restrict a comprehensive understanding of all muscular adaptations, it was a conscious trade-off to maintain a minimally invasive and practical setup. Interestingly, the results suggest that even with this reduced set of sensors, it is possible to robustly estimate Achilles tendon offloading. This supports the idea that minimal sensing strategies could be effective for clinical or wearable deployment, where sensor economy is critical.

7.1 Future Directions

Validating CMC–EMG Estimations

The Achilles tendon force estimations in this study relied on the Computed Muscle Control (CMC) algorithm in OpenSim, informed by experimental EMG. Although OpenSim is a globally recognized and validated modeling framework, the specific performance of the CMC–EMG-informed approach in predicting tendon loading has not been explicitly validated in our context.

A promising direction for future work is to design targeted validation experiments. For instance, a controlled walking task could be performed by a therapist or subject under two conditions: (1) normative gait and (2) deliberate co-contraction of antagonist muscle groups. In such a scenario, we would expect a significant increase in estimated tendon loading from the EMG-informed CMC pipeline due to increased muscular effort, while the standard CMC pipeline (without EMG input) may not show this increase. Observing such divergence would strengthen confidence in the EMG-informed model's sensitivity and accuracy in estimating internal loads.

Beyond EMG as Sole Evidence of AFO Effectiveness

It is important to emphasize that a reduction in EMG amplitude alone is not sufficient to claim effective mechanical offloading by the AFO. Muscle activation can decrease

due to a variety of factors, such as altered neural strategies or compensation, without necessarily reflecting a corresponding change in joint or tendon loading. That is why our multi-modal approach, combining EMG analysis with tendon force estimation, is crucial. Future studies should continue integrating mechanical and neuromuscular indicators to holistically assess the performance of assistive devices.

Chapter 8

Conclusions

Understanding the dynamics of muscle–tendon units (MTUs) plays a crucial role in numerous fields, including injury prevention, rehabilitation, sports science, ergonomic design, assistive technologies, and clinical diagnostics. In rehabilitation and preventive care, detecting abnormal muscle forces allows for the design of more effective interventions aimed at reducing injury risk and promoting safe recovery. In sports science, optimizing MTU behavior not only enhances athletic performance but also accelerates recovery and mitigates the risk of re-injury, especially given the high incidence of tendon-related injuries in athletes. Clinical applications further benefit from MTU analysis, aiding in the diagnosis of neuromuscular disorders and supporting surgical planning and post-operative recovery.

This study explored the biomechanical and neuromuscular impact of powered ankle–foot orthoses (AFOs) on lower limb function, with a specific focus on triceps surae muscle activity and Achilles tendon loading during walking. By integrating experimental data with advanced musculoskeletal (MSK) simulations, we demonstrated the potential of active AFOs to reduce muscular workload and tendon forces, particularly during the push-off phase of gait.

Surface electromyography (EMG) recordings consistently showed reduced activation levels in the soleus and gastrocnemii muscles as AFO assistance increased. These findings indicate that active torque support provided by the Dephy ExoBoot effectively offloads the plantarflexor muscles. Supporting this evidence, OpenSim simulations revealed a reduction in muscle-generated ankle moments and Achilles tendon force across increasing assistance levels. These converging results underscore the functional contribution of powered AFOs in supporting locomotion and their promising therapeutic potential in rehabilitation settings.

Beyond localized effects, this study contributes to a broader understanding of how wearable robotic devices interact with human biomechanics. Through a rigorous validation of simulation outputs, including inverse kinematics, joint angle comparisons (MyoSuite, OpenSim, and Visual3D), and analysis of muscle and tendon loading, we have confirmed the reliability of our integrated modeling approach. This includes a thorough examination of signal alignment, gait segmentation, and individualized assistance response across subjects and walking speeds.

Importantly, this work demonstrates that MSK modeling can serve as a powerful non-invasive alternative to traditional invasive measurement methods for studying MTU dynamics. Our framework enables the isolation of individual joint and muscle contributions and supports the virtual testing of assistive device parameters before clinical implementation. Such tools can enhance the design and personalization of rehabilitation protocols, ultimately improving functional outcomes for patients recovering from injury or surgery.

In summary, the outcomes of this thesis offer several key insights:

- Active AFOs significantly reduce plantarflexor muscle activation and Achilles tendon force during the push-off phase, confirmed by both EMG and simulation data.
- Simulation results closely align with experimental data, supporting the use of EMG-informed MSK modeling to estimate internal biomechanical variables.
- The reduction of EMG activity alone is insufficient to evaluate device effectiveness; tendon force estimations provide a more comprehensive assessment of mechanical unloading.
- The integration of minimal sensor data (4 EMG channels per leg) proved sufficient for effective modeling and evaluation, suggesting a feasible path for future wearable implementations.
- Model validation steps, including torque profile matching and cross-platform kinematics comparison, confirmed the robustness of the pipeline.

Outlook and Future Work

While this study provides strong evidence of the assistive effects of powered AFOs, several limitations must be acknowledged, such as the idealized actuator modeling, treadmill-based data collection, simplified EMG normalization, and limited muscle recordings. These aspects provide opportunities for improvement in future research.

Additionally, future work should focus on further validating EMG-informed simulations by evaluating their sensitivity to physiological changes, such as co-contraction strategies. Testing under controlled walking tasks with varying muscle activation profiles (e.g., with and without deliberate co-contraction) could help confirm that tendon force estimates truly reflect underlying neuromuscular control.

Ultimately, this research sets the stage for developing more accurate, efficient, and personalized rehabilitation strategies. By leveraging MSK modeling, we can move toward designing assistive devices and therapeutic protocols that are both patient-specific and clinically effective, with the long-term goal of improving mobility, reducing recovery time, and enhancing quality of life.

Appendix A

Appendix A

A.1 Evaluation Metrics

This section reports the mathematical definitions of the evaluation metrics used to compare simulation outcomes across platforms.

Root Mean Square Error (RMSE)

$$\text{RMSE} = \sqrt{\frac{1}{N}\sum_{i=1}^{N}(x_i - y_i)^2} \tag{A.1}$$

Measures the average squared difference between two signals x_i and y_i (e.g., MyoSuite vs. Visual3D) across N samples. Lower values indicate greater similarity.

Normalized RMSE (NRMSE)

$$\text{NRMSE} = \frac{\text{RMSE}}{\max(y) - \min(y)} \times 100 \tag{A.2}$$

The RMSE normalized to the range of the reference signal y. Expressed as a percentage, it enables comparisons across signals with different scales.

Coefficient of Multiple Correlation (CMC)

$$\text{CMC} = \sqrt{1 - \frac{\sum_{i=1}^{N}\sum_{j=1}^{M}(x_{ij} - \bar{x}_j)^2}{\sum_{i=1}^{N}\sum_{j=1}^{M}(x_{ij} - \bar{x})^2}} \tag{A.3}$$

Evaluates the similarity between multiple waveforms x_{ij} (e.g., different gait cycles or subjects) and their average $\bar{x}_j$. Ranges from 0 to 1; values closer to 1 indicate higher similarity.

Range of Motion (ROM)

$$\text{ROM} = \max(x) - \min(x) \tag{A.4}$$

Defines the joint angular excursion during a gait cycle. Expressed in degrees.

ROM Error

$$\text{ROM Error} = |\text{ROM}_{\text{model}} - \text{ROM}_{\text{reference}}| \tag{A.5}$$

Absolute difference between the ROM estimated by the model and that from the reference. Evaluates how well the model captures the joint dynamics.

Root Mean Square (RMS)

$$\text{RMS} = \sqrt{\frac{1}{N}\sum_{i=1}^{N} x_i^2} \tag{A.6}$$

Used to estimate the average power of a signal (e.g., muscle activation or EMG envelope).

Peak Reduction (%)

$$\text{Peak Reduction} = \frac{P_{\text{baseline}} - P_{\text{condition}}}{P_{\text{baseline}}} \times 100 \tag{A.7}$$

Percentage reduction of the peak value (e.g., tendon force or activation) compared to a baseline condition. Quantifies the unloading or assistance effect.

Bibliography

[1] M. Wong, A.H. Jardaly, and J. Kiel. "Anatomy, Bony Pelvis and Lower Limb: Achilles Tendon". In: *StatPearls [Internet]*. [Updated 2023 Aug 8]. Treasure Island (FL): StatPearls Publishing, 2025. URL: https://www.ncbi.nlm.nih.gov/books/NBK499917/ (cit. on p. 4).

[2] Andrew G. Shamrock, Megan A. Dreyer, and Matthew A. Varacallo. *Achilles Tendon Rupture*. StatPearls [Internet]. Updated 2023 Aug 17. Treasure Island (FL): StatPearls Publishing, 2025. URL: https://www.ncbi.nlm.nih.gov/books/NBK430844/ (cit. on p. 4).

[3] Jonathan Thompson and Bob Baravarian. "Acute and Chronic Achilles Tendon Ruptures in Athletes". In: *Clinics in Podiatric Medicine and Surgery* 28.1 (2011). Foot and Ankle Athletic Injuries, pp. 117–135. ISSN: 0891-8422. DOI: https://doi.org/10.1016/j.cpm.2010.10.002. URL: https://www.sciencedirect.com/science/article/pii/S0891842210000984 (cit. on pp. 4, 5).

[4] A. J. Carr and S. H. Norris. "The blood supply of the calcaneal tendon". In: *The Journal of Bone and Joint Surgery. British Volume* 71.1 (1989), pp. 100–101. DOI: 10.1302/0301-620X.71B1.2914976 (cit. on p. 4).

[5] Jonas Rubenson, Nathan J. Pires, Hiu On Loi, Gordon J. Pinniger, and David G. Shannon. "On the ascent: the soleus operating length is conserved to the ascending limb of the force-length curve across gait mechanics in humans". In: *Journal of Experimental Biology* 215.Pt 20 (Oct. 2012). Epub 2012 Jul 5, pp. 3539–3551. DOI: 10.1242/jeb.070466 (cit. on p. 5).

[6] Masaki Ishikawa, Paavo V. Komi, Michael J. Grey, Vesa Lepola, and Gert-Peter Brüggemann. "Muscle-tendon interaction and elastic energy usage in human walking". In: *Journal of Applied Physiology (1985)* 99.2 (Aug. 2005). Epub 2005 Apr 21, pp. 603–608. DOI: 10.1152/japplphysiol.00189.2005 (cit. on p. 5).

[7] B. Meulenkamp, D. Stacey, D. Fergusson, B. Hutton, R. S. Mlis, and I. D. Graham. "Protocol for treatment of Achilles tendon ruptures: a systematic review with network meta-analysis". In: *Systematic Reviews* 7.1 (Dec. 2018), p. 247. DOI: 10.1186/s13643-018-0903-5 (cit. on p. 5).

[8] Heath P. Gould, Joseph M. Bano, Jennifer L. Akman, and Allison L. Fillar. "Postoperative Rehabilitation Following Achilles Tendon Repair: A Systematic Review". In: *Sports Medicine and Arthroscopy Review* 29.2 (June 2021), pp. 130–145. DOI: 10.1097/JSA.0000000000000309 (cit. on p. 5).

[9] Rachel W. Jackson and Steven H. Collins. "An experimental comparison of the relative benefits of work and torque assistance in ankle exoskeletons". In: *Journal of Applied Physiology* 119.5 (2015), pp. 541–557. DOI: 10.1152/japplphysiol.01133.2014 (cit. on p. 5).

[10] Philippe Malcolm, Wim Derave, Samuel Galle, and Dirk De Clercq. "A Simple Exoskeleton That Assists Plantarflexion Can Reduce the Metabolic Cost of Human Walking". In: *PLOS ONE* 8.2 (Feb. 2013), pp. 1–7. DOI: 10.1371/journal.pone.0056137. URL: https://doi.org/10.1371/journal.pone.0056137 (cit. on p. 5).

[11] Karin G. Silbernagel, Roland Thomeé, Bengt I. Eriksson, and Jon Karlsson. "Continued sports activity, using a pain-monitoring model, during rehabilitation in patients with Achilles tendinopathy: a randomized controlled study". In: *The American Journal of Sports Medicine* 35.6 (June 2007), pp. 897–906. DOI: 10.1177/0363546506298279 (cit. on p. 5).

[12] David Condie and C.B. Meadows. "Some biomechanical considerations in the design of ankle-foot orthoses". In: 31 (Jan. 1977) (cit. on p. 5).

[13] Steven H. Collins, M. Bruce Wiggin, and Gregory S. Sawicki. "Reducing the Energy Cost of Human Walking Using an Unpowered Exoskeleton". In: *Nature* 522 (2015), pp. 212–215. DOI: 10.1038/nature14288 (cit. on p. 5).

[14] Annegret Mündermann, Christopher O. Dyrby, Darryl D. D'Lima, Clifford W. Jr. Colwell, and Thomas P. Andriacchi. "In vivo knee loading characteristics during activities of daily living as measured by an instrumented total knee replacement". In: *Journal of Orthopaedic Research* 26.9 (Sept. 2008), pp. 1167–1172. DOI: 10.1002/jor.20655 (cit. on p. 6).

[15] Taylor JM Dick, Allison S Arnold, and James M Wakeling. "Quantifying Achilles tendon force in vivo from ultrasound images". In: *Journal of Biomechanics* 49.14 (2016), pp. 3200–3207. DOI: 10.1016/j.jbiomech.2016.07.036 (cit. on p. 6).

[16] Emily M Keuler, Isaac F Loegering, Jack A Martin, Joshua D Roth, and Darryl G Thelen. "Shear wave predictions of Achilles tendon loading during human walking". In: *Scientific Reports* 9.1 (2019), p. 13419. DOI: 10.1038/s41598-019-49063-7 (cit. on p. 6).

[17] Nicholas B Bolus, Hyeon Ki Jeong, Bradley M Blaho, Mohsen Safaei, Aaron J Young, and Omer T Inan. "Fit to Burst: Toward Noninvasive Estimation of Achilles Tendon Load Using Burst Vibrations". In: *IEEE Transactions on Biomedical Engineering* (2020). Early access. DOI: 10.1109/TBME.2020.3005353 (cit. on p. 6).

[18] A. Rajagopal, C. L. Dembia, M. S. DeMers, D. D. Delp, J. L. Hicks, and S. L. Delp. "Full-Body Musculoskeletal Model for Muscle-Driven Simulation of Human Gait". In: *IEEE Transactions on Biomedical Engineering* 63.10 (Oct. 2016), pp. 2068–2079. DOI: 10.1109/TBME.2016.2586891 (cit. on pp. 6, 31).

[19] Dong Sun, Gusztáv Fekete, Julien S. Baker, Qichang Mei, Bíró István, Yan Zhang, and Yaodong Gu. "A Pilot Study of Musculoskeletal Abnormalities in Patients in Recovery from a Unilateral Rupture-Repaired Achilles Tendon". In: *International Journal of Environmental Research and Public Health* 17.13 (2020). ISSN: 1660-4601. DOI: 10.3390/ijerph17134642. URL: https://www.mdpi.com/1660-4601/17/13/4642 (cit. on p. 7).

[20] Scott L. Delp, Frank C. Anderson, Allison S. Arnold, Peter Loan, Ayman Habib, Chand T. John, Eran Guendelman, and Darryl G. Thelen. "OpenSim: Open-Source Software to Create and Analyze Dynamic Simulations of Movement". In: *IEEE Transactions on Biomedical Engineering* 54.11 (2007), pp. 1940–1950. DOI: 10.1109/TBME.2007.901024 (cit. on pp. 7, 32).

[21] Dong Sun, Gusztáv Fekete, Julien S. Baker, Qichang Mei, István Bíró, Yan Zhang, and Yaodong Gu. "A Pilot Study of Musculoskeletal Abnormalities in Patients in Recovery from a Unilateral Rupture-Repaired Achilles Tendon". In: *International Journal of Environmental Research and Public Health* 19.23 (2022), p. 15965. DOI: 10.3390/ijerph192315965 (cit. on p. 7).

[22] Meta AI. *MyoSuite*. Accessed: 2025-06-04. 2022. URL: https://sites.google.com/view/myosuite (cit. on p. 7).

[23] Vittorio Caggiano, Huawei Wang, Guillaume Durandau, Massimo Sartori, and Vikash Kumar. *MyoSuite – A contact-rich simulation suite for musculoskeletal motor control*. https://github.com/MyoHub/myosuite. 2022. DOI: 10.48550/ARXIV.2205.13600. URL: https://sites.google.com/view/myosuite (cit. on pp. 7, 17, 27).

[24] Dephy, Inc. *Dephy – Advancing Human Performance*. Accessed: 2025-06-04. 2024. URL: https://www.dephy.com (cit. on pp. 8, 16).

[25] Vicon Motion Systems Ltd. *Vicon: Award Winning Motion Capture Systems*. https://www.vicon.com. Accessed: 2025-06-12. 2025 (cit. on p. 11).

[26] HAS-Motion Software Documentation. *Plug-In Gait Full-Body (Visual3D Tutorial)*. https://wiki.has-motion.com/doku.php?id=visual3d:tutorials:modeling:plug-in_gait_full-body. Accessed: 2025-06-13. 2025 (cit. on pp. 12, 22).

[27] HAS-Motion Software Documentation. *IOR Gait Full Body Model (Visual3D Tutorial)*. https://wiki.has-motion.com/doku.php?id=visual3d:tutorials:modeling:ior_gait_full_body_model. Last modified: 2025-03-10; accessed: 2025-06-13. 2025 (cit. on pp. 12, 22).

[28] Delsys Inc. *Trigno® Wireless Biofeedback System User's Guide*. Accessed: 2025-06-13. Delsys Inc. Natick, MA, USA, 2025 (cit. on p. 14).

[29] Ajay Seth et al. "OpenSim: Simulating musculoskeletal dynamics and neuromuscular control to study human and animal movement". In: *PLoS Computational Biology* 14.7 (2018), e1006223. DOI: 10.1371/journal.pcbi.1006223. URL: https://doi.org/10.1371/journal.pcbi.1006223 (cit. on p. 16).

[30] C-Motion, Inc. *Visual3D – 3D biomechanical analysis software*. http://www.c-motion.com/visual3d. Accessed: 2025-06-13. 2025 (cit. on p. 17).

[31] M.R. Yeadon. "The simulation of aerial movement—II. A mathematical inertia model of the human body". In: *Journal of Biomechanics* 23.1 (1990), pp. 67–74. ISSN: 0021-9290. DOI: https://doi.org/10.1016/0021-9290(90)90370-I. URL: https://www.sciencedirect.com/science/article/pii/002192909090370I (cit. on p. 24).

[32] Caggiano, Vittorio and La Barbera, Vittorio and Kumar, Vikash. *MyoModel: Library of Musculoskeletal Models*. https://github.com/myolab/myo_model. GitHub repository (accessed: 2025-06-13). 2024 (cit. on p. 27).

[33] Vittorio Caggiano, Huawei Wang, Guillaume Durandau, Massimo Sartori, and Vikash Kumar. *MyoSim: Musculoskeletal Models in MuJoCo*. https://github.com/MyoHub/myo_sim. GitHub repository (accessed: 2025-06-13). 2022–2025 (cit. on p. 27).

[34] MyoHub authors. *Inverse Dynamics Tutorial (Jupyter Notebook)*. https://github.com/MyoHub/myosuite/blob/main/docs/source/tutorials/6_Inverse_Dynamics.ipynb. GitHub Jupyter notebook (accessed: 2025-06-13). 2025 (cit. on p. 28).

[35] Edith M. Arnold, Samuel R. Ward, Richard L. Lieber, and Scott L. Delp. "A model of the lower limb for analysis of human movement". In: *Annals of Biomedical Engineering* 38.2 (2010), pp. 269–279. DOI: 10.1007/s10439-009-9852-5 (cit. on pp. 32, 47).

[36] R. Hara, J. McGinley, C. Briggs, et al. "Predicting the location of the hip joint centres, impact of age group and sex". In: *Scientific Reports* 6 (2016), p. 37707. DOI: 10.1038/srep37707 (cit. on p. 46).

[37] MP Kadaba, HK Ramakrishnan, and ME Wootten. "Repeatability of kinematic, kinetic, and electromyographic data in normal adult gait". In: *Journal of Orthopaedic Research* 7.6 (1989), pp. 849–860 (cit. on p. 47).

[38] M. S. Zahedi, W. D. Spence, S. E. Solomonidis, and J. P. Paul. "Repeatability of kinetic and kinematic measurements in gait studies of the lower limb amputee". In: *Prosthetics and Orthotics International* 11.2 (Aug. 1987), pp. 55–64. DOI: 10.3109/03093648709078179 (cit. on p. 47).

[39] A. S. Fox, J. Bonacci, J. Warmenhoven, and M. F. Keast. "Measurement error associated with gait cycle selection in treadmill running at various speeds". In: *PeerJ* 11 (Mar. 2023), e14921. DOI: 10.7717/peerj.14921 (cit. on p. 47).

[40] Massimo Sartori, Dario Farina, and David G Lloyd. "EMG-driven forward-dynamic estimation of muscle force and joint moment about multiple degrees of freedom in the human lower extremity". In: *PLoS One* 7.12 (2012), e52618 (cit. on pp. 48, 59).

[41] A. J. Meyer, C. Patten, and B. J. Fregly. "Lower extremity EMG-driven modeling of walking with automated adjustment of musculoskeletal geometry". In: *PLoS One* 12.7 (July 2017), e0179698. DOI: 10.1371/journal.pone.0179698 (cit. on pp. 48, 59).

[42] Samuel Galle, Philippe Malcolm, Wim Derave, and Dirk De Clercq. "Adaptation to walking with an exoskeleton that assists ankle extension". In: *Gait & Posture* 50 (2017), pp. 1–9. DOI: 10.1016/j.gaitpost.2016.08.020 (cit. on p. 59).

[43] Gregory S. Sawicki, Owen N. Beck, Ilhyun Kang, and Aaron J. Young. "The exoskeleton expansion: improving walking and running economy". In: *Journal of NeuroEngineering and Rehabilitation* 17.1 (2020), pp. 1–9. DOI: 10.1186/s12984-020-00701-5 (cit. on p. 59).